Cumulative Results of Extended Forecast Experiments II: Model Performance for Summer Cases

K. MIYAKODA, G. D. HEMBREE AND R. F. STRICKLER

Geophysical Fluid Dynamics Laboratory/NOAA, Princeton University, Princeton, NJ 08540

(Manuscript received 6 June 1978, in final form 10 January 1979)

ABSTRACT

Two-week experimental forecasts were carried for 12 July cases with a nine vertical level, 270 km grid-size hemispheric model, and the results were examined statistically. The solutions studied were the stationary (10-day average) and transient components of the general circulation; in particular, the ensemble mean of temperature, zonal wind and eddy kinetic energy; and the hemispheric maps of ensemble mean height fields. The predictive ability of this model was examined by comparing the results with observation and calculating statistical scores such as standard deviation, correlation coefficient and horizontal gradient ($S1$) score for 1000, 500 and 50 mb geopotential height verified against the NMC (National Meteorological Center) analysis. The results were also analyzed in terms of zonal wavenumbers of geopotential. So far as this model (1967 version) is concerned, the predictability in the lower atmosphere seems to decay more rapidly in July than in January. However, the predictability of the middle and upper troposphere is greater in July than in January; the planetary-scale waves were better predicted. The simulation of the summer stratosphere is very poor with the nine-level vertical resolution. The prediction was also compared with that of a spectral model of comparable horizontal and vertical resolution.

1. Introduction

This is the second of a series of papers on weather prediction experiments for the time range of two weeks. Part I (Miyakoda *et al.*, 1972) was a report for 12 January cases, whereas Part II is for July cases.

The prediction model, referred to as the "GFDL 1967 version" (Geophysical Fluid Dynamics Laboratory), was originally constructed for general circulation (GC) studies and was adapted in 1967 as a benchmark model for real-data simulation. The model covers a hemispheric domain with horizontal resolution of $N40$ (N is the number of grid points between the pole and equator) and of nine vertical levels. The prediction model and the initialization of data were exactly the same as in Part I except that radiation parameters, sea surface temperature, sea-ice limit and sea-ice temperature are adjusted to the month of July in Part II. Refer to Part I and also Miyakoda (1973) for a detailed description of the model, the initialization and the verification.

Since this project started in 1967, more than 10 years have passed. Although this work was thought important, the cases were run as a backup in the computer schedule and there were also gaps in computer availability for this experiment between 1972 and 1974. During this whole period, the forecasting model has been totally frozen, though the computer codes have been modified frequently according to the change of machines and software. Fortunately, this project has been carried to this extent, and we are now able to present the contrasts between the warm and the cold season forecasts. It may be of particular interest to see whether the summer situations are, indeed, more difficult to forecast than the winter.

The manner of presentation of results in this paper is almost the same as in Part I. First will be shown the 10-day average and transient circulation features; second, verification scores; and third, a spectral analysis of the model's forecasts. The performance of the precipitation simulation and forecasts will be discussed in a separate paper.

The last decade was an important period for extended-range forecasts in which the limit of predictability with the deterministic numerical weather forecasts have been critically and extensively tested. Although there was no drastic change on the scope of the predictability, knowledge on the medium-range forecasts has been remarkably extended, and the technology on the weather forecast models has been considerably advanced. A comparison will be shown in this paper between a forecast with this model and that with a recent spectral model (Gordon and Stern, 1974). The latter model requires 16 min for a 1-day forecast with the Texas Instruments ASC, while the GFDL 1967 version needs 48 min with the ASC. In the last part of this paper, summarizing the results of Parts I and II, comments

TABLE 1. Initial day for cases used (1200 GMT).

27 June 1965	1 July 1968
16 July 1965	16 July 1968
3 July 1966	2 July 1969
17 July 1966	19 July 1969
2 July 1967	2 July 1970
17 July 1967	16 July 1970

will be given on the model employed in this study and the future improvement.

2. Cases

Twelve cases all for July (except three days in June and two days in August) were selected randomly from a six-year period (1965–70), two cases each year (Table 1).

The initial and verification data were taken from NMC analyses for geopotential, temperature and moisture. However, the initial conditions of moisture only were analyzed in our laboratory (GFDL) through an objective analysis process (see Oort and Rasmusson, 1971). Half of the NMC data were supplied by NCAR (National Center for Atmospheric Research) archives (Jenne, 1975) and half from the Climatic Data Center, NOAA, at Asheville, North Carolina.

3. General circulation features

The predicted and observed temperature, zonal wind and eddy kinetic energy were averaged zonally and temporally over the last 10 days in each forecast period, and then ensemble-averaged over different years. The observed analysis is only valid north of 15°.

a. Temperature

Fig. 1 is the height-latitude chart (meridional section) of predicted temperature and its difference from observed temperature. The agreement between prediction and observation is close enough that visual detection of discrepancy is difficult. Therefore, the difference is shown in Fig. 1B. An inspection of these figures leads to the following conclusions:

1) The predicted temperature is higher than the observed temperature in the entire lower stratosphere and half of the troposphere within and near the tropics. This tendency is just the opposite to that in January. This lends support to the hypothesis that the prohibition of interhemispheric exchange of heat due to the equatorial "wall" is one of the causes for the higher temperature in the model's summer hemisphere.

2) However, the predicted troposphere in the extratropics is colder than the observation. This feature of cooling resembles that of January cases. Interestingly, the same tendency was also noted in the GISS model [Goddard Institute of Space Studies (Druyan *et al.*, 1975)].[1] These shortcomings (GFDL and GISS) may come from the insufficient poleward heat transport by eddy motions and insufficient downward motion due to lack of vertical resolution in this model (Mahlman, personal communication) and also from an incomplete specification of cloud coverage in high latitudes. [The GISS model is different in this respect, however (see Somerville *et al.*, 1974).]

3) In the layer next to the earth's surface, there is a region of positive error around 55°N. This feature is common in the January case, though the latitudinal position is different.

[1] The NCAR model (NCAR, 1975) had also the excessive cooling (about 10°C) but in the tropical troposphere.

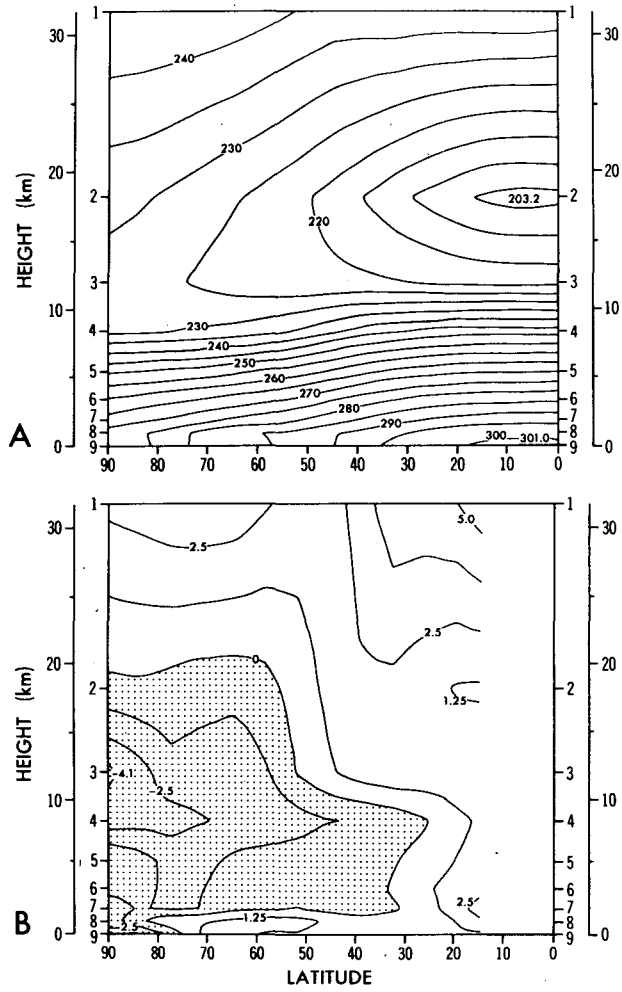

FIG. 1. Height-latitude chart of (A) predicted temperature (K) and (B) temperature error (K) i.e., the predicted temperature minus the observed; the negative region is stippled. The ordinate is geometric height (km) and the nine levels in the model.

b. Zonal wind

There is general agreement between prediction and observation (Fig. 2). Note that the maximum value in our "observation" is very slightly different from that of Oort and Rasmusson (1971). Discrepancies between the model and the observation are found in the following points.

1) Predicted midlatitude westerlies penetrate excessively from the troposphere into the stratosphere. This shortcoming is anticipated due to lack of vertical resolution in the model.

2) The intensity of predicted polar westerlies at about 80°N is substantially weaker probably due to the insufficient space resolution.

3) The midlatitude westerlies in the model are protruded appreciably toward the doldrums. This corresponds to the fact that the subtropical highs in the prediction are weaker (see Fig. 5). A defective

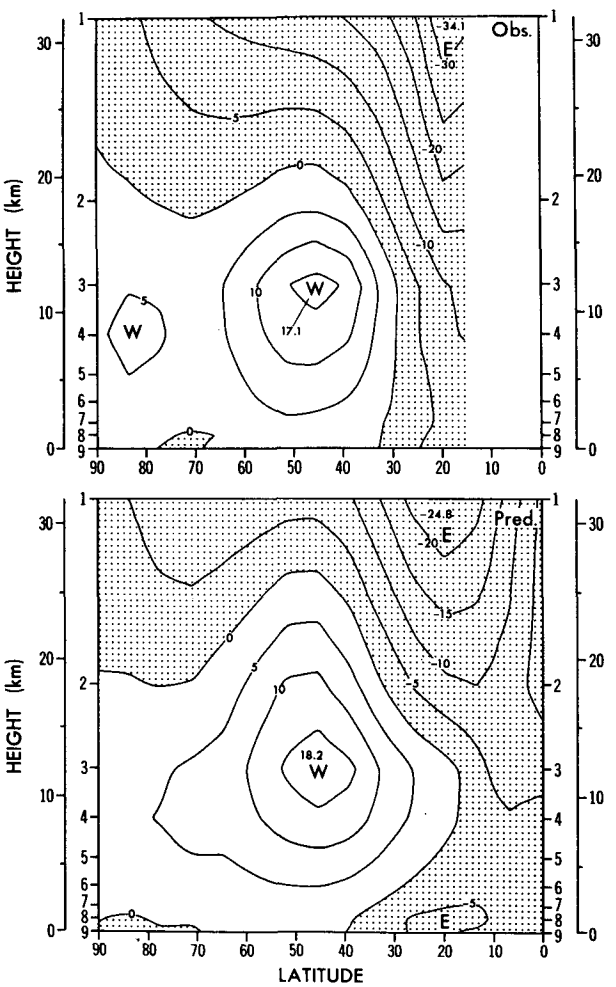

FIG. 2. Height-latitude chart of observed and predicted zonal wind (m s^{-1}). The regions of easterlies are stippled. Extreme values are plotted.

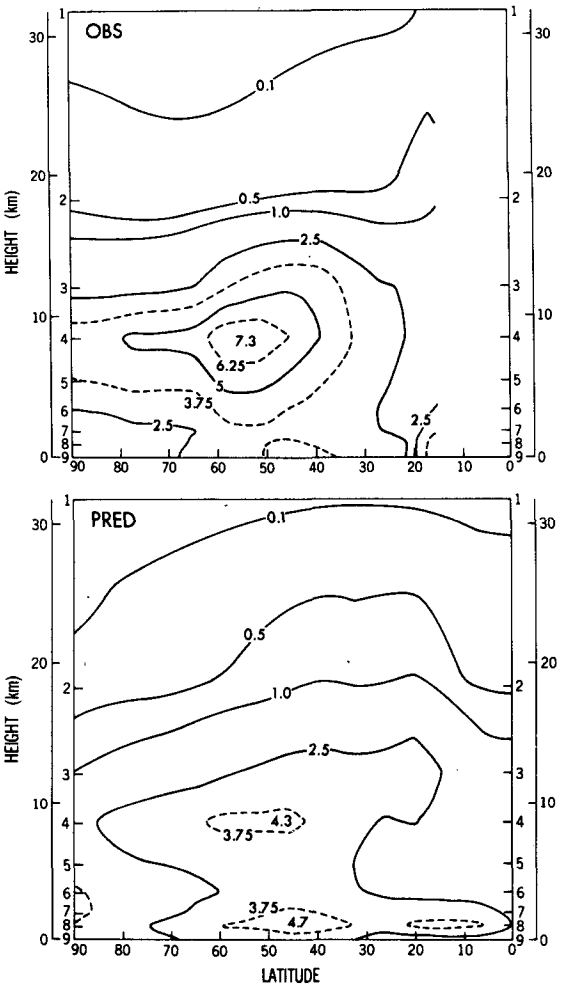

FIG. 3. Height-latitude chart of observed and predicted eddy kinetic energy (10^{-5} J cm^{-3}). The maxima are plotted.

specification of soil moisture is considered to be responsible for it. The latitudinal position of the predicted subtropical jet coincides well with that of the observed; this is not the case in the winter forecasts.

4) The predicted midlatitude jet at the tropopause level is more intense than the observed. As was discussed in Part I, this feature may be associated with the omission of vertical diffusion in the upper half of the model atmosphere. [See Stone *et al.* (1977), in which the intensity of the July jet was properly simulated.]

c. Eddy kinetic energy

Fig. 3 is the eddy kinetic energy KE = $\frac{1}{2}\rho_0(\overline{u'^2} + \overline{v'^2})$, where u' and v' are deviations from the zonal means and ρ_0 is the air density of the standard atmosphere. The most outstanding feature is that the model KE is very much weaker than the observed. The intensity of computed KE at its maximum posi-

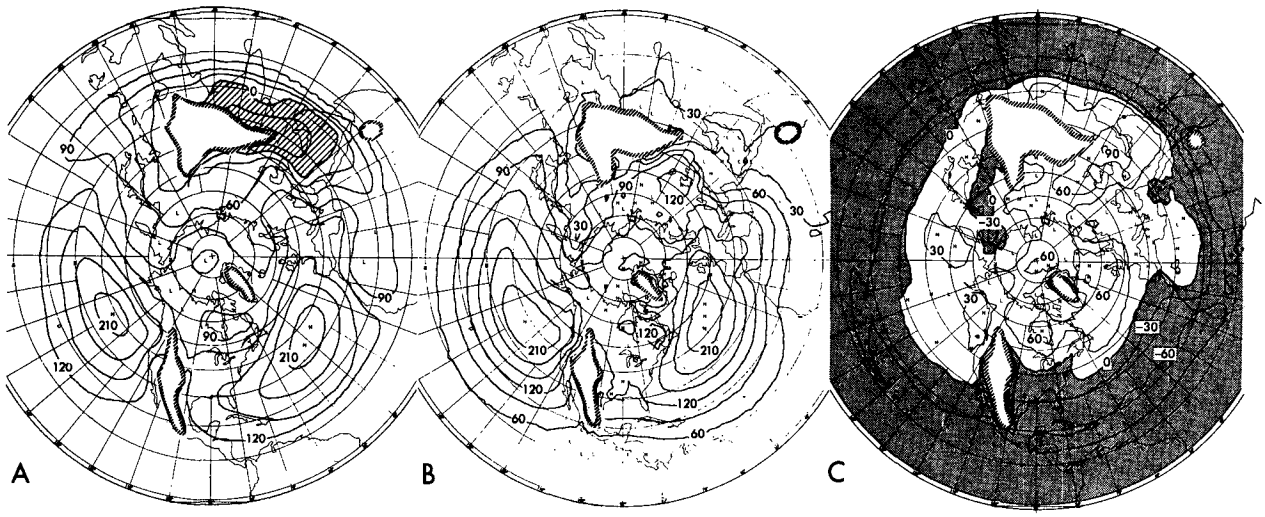

FIG. 4. Observed (A) and predicted (B) mean maps of 1000 mb geopotential heights, negative regions shaded, and the error map (C) (i.e., the predicted minus the observed). Contours in all maps are at 30 m intervals. Negative areas of height error in (C) are shaded. The loci of small segmented lines mark the mountain areas.

tion is lower by 41% than that of the observed, in contrast to the 25% reduction in the case of January. The secondary maximum that is associated with the polar frontal jet was not well-produced. The major cause for these deficiencies is the coarse-grid resolution of the model for both horizontal and vertical directions and, in part, the excessive horizontal diffusion. Compared with January, July has an appreciably reduced intensity of KE both in the observations and predictions, indicating that the baroclinic process in the middle latitudes is inactive in summer and also reflecting the fact that the cyclone generation is less.

d. Hemispheric geopotential fields

Height fields both for the observation and the prediction averaged for 10 days and over 12 cases are shown in Figs. 4 and 5, together with their forecast errors $\delta Z = Z$ pred $- Z$ obs. The observed patterns in these figures closely resemble the climatological maps obtained by Crutcher and Jenne (1970).

In the 1000 mb map, the height error is positive toward the pole and negative toward the equator with a node near 30°N. The largest error is found between Turkestan and the Himalayas, and also over the North Sea and northern Canada. The former error may largely be due to improper heat balance at the surface and also related to the model's weakness in simulating capability of the Asian monsoon, which comes from the prohibited interhemispheric exchange over the Indian Ocean. In fact, the global models of Manabe and Holloway (1975) and Stone *et al.* (1977) successfully simulated the pattern east of the Caspian Sea (though Manabe

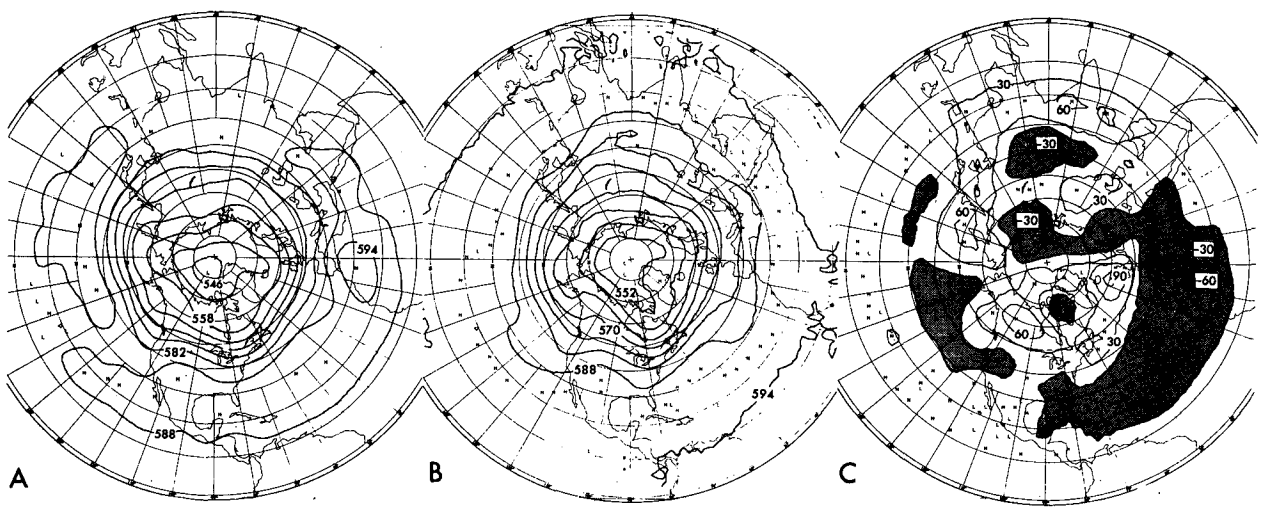

FIG. 5. As in Fig. 4 for 500 mb except mean height contours are at 60 m intervals and height error contours are at 30 m intervals.

and Holloway's map was the sea level pressure for June, July and August.) The latter error over northern Canada might be associated with an inadequate treatment of surface heat balance. The global model's performances were no better than the present result. It is interesting to note that in our result there is a large negative error zone originating from the Himalayas, extending downstream and reaching the Kamchatka Peninsula; a similar tendency may be noticed, to a lesser extent, in the lee of Rockies. Note that this feature did not occur (or was not detectable) in the January case. As was pointed out by Reed and Kunkel (1960), the arctic in summer is not dominated by a semi-permanent anticyclone, which is different from a classical picture of the atmospheric general circulation.

At 500 mb, there are five major stationary troughs in the observation. Some predicted troughs agree well in longitudinal positions with the observed troughs and others do not. Particularly, a trough over Siberia is missing, and the predicted Icelandic and Aleutian troughs are shifted eastward. Another glaring error is that a high belt (at ~30°N, which corresponds to Pacific and Atlantic subtropical highs) does not exist in the predicted map and the maximum of geopotential is found at the equator. In view of the fact that global GC models had a similar defect (e.g., Manabe *et al.*, 1974; Stone *et al.*, 1977), the cause of this bias may not be ascribed to the equatorial "wall" but possibly to the insufficient horizontal resolution. Over the Sahara desert, the error is particularly large at 500 mb. Different from other subtropical high regions, there is a high in the observed map at 500 mb but a low at 1000 mb, which is usually ascribed to the extreme heating over northern Africa (Burpee, 1972). The deficiency in our result, therefore, is related to the improper treatment of the desert, particularly soil moisture. In this model, the availability of soil moisture was simply specified to be 0.5 over all land areas; this

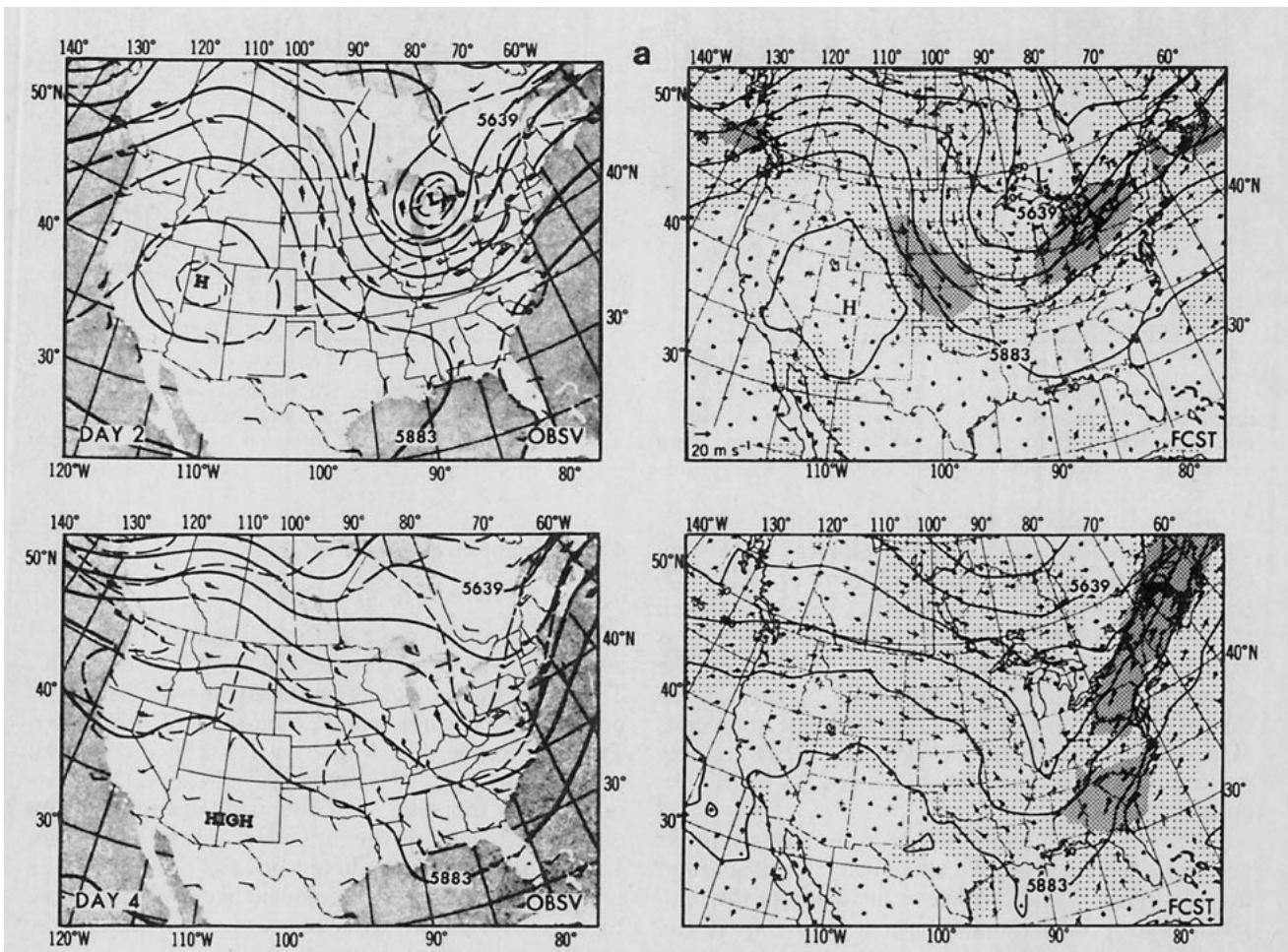

FIG. 6a. Forecast and observed 500 mb height maps for days 2 and 4 for the case beginning 1200 GMT 2 July 1970. Observed charts are from the daily weather maps of the National Oceanic and Atmospheric Administration. The contour interval is 61 m. For the observed maps the wind speed is in knots with a full barb indicating 10 kt and a flag 50 kt. On the forecast maps wind speed (m s^{-1}) is shown by the length of the arrow. Isotachs are shown by shading with light shading 10–20 m s^{-1} and dark shading for speeds >30 m s^{-1}.

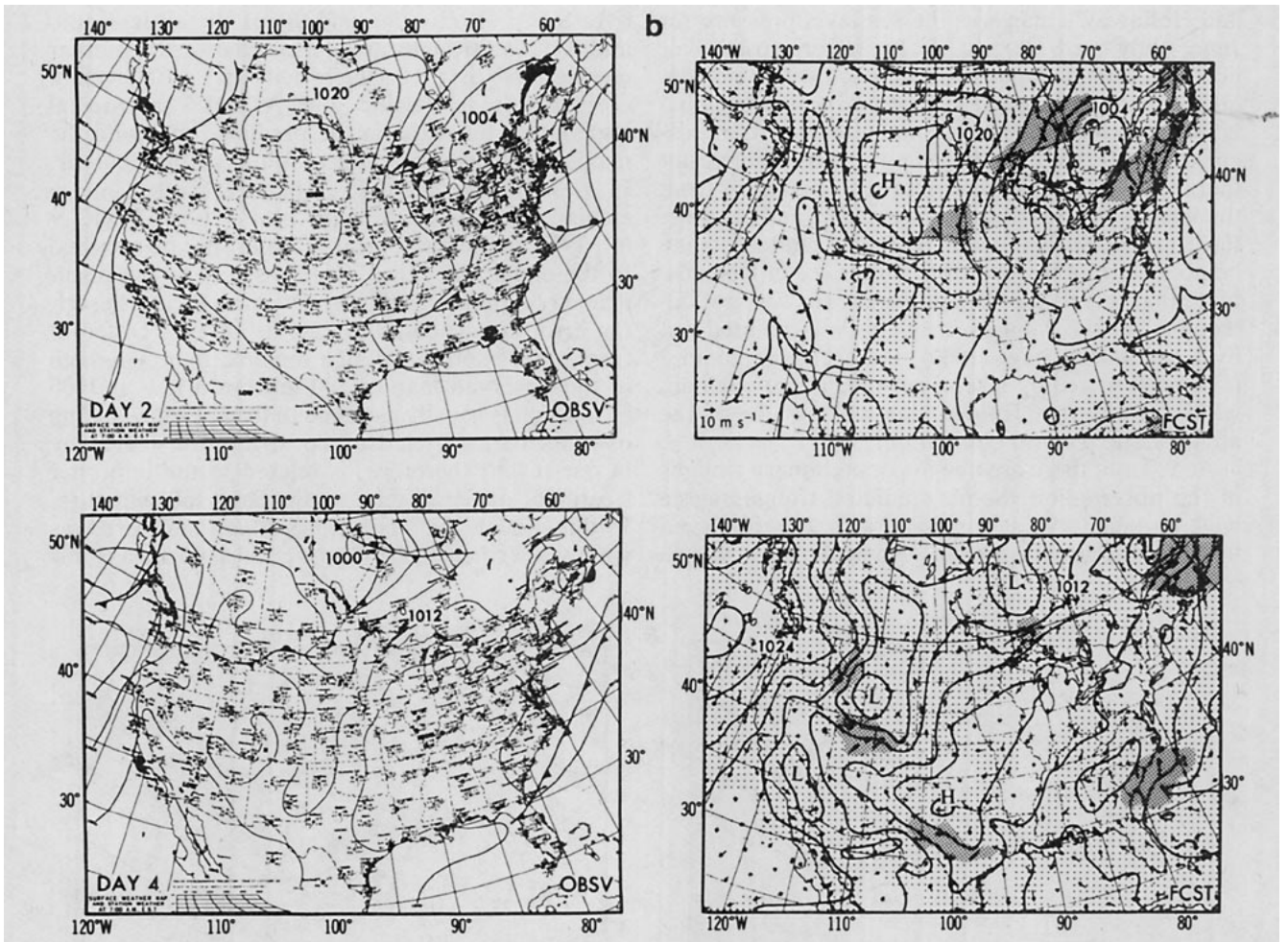

FIG. 6b. As in Fig. 6a but for the sea level pressure maps. The contour interval is 4 mb. For the observed maps areas of precipitation are shaded. The surface wind is in knots with each full barb indicating 10 kt. On the forecast maps the winds for the lowest model level (~70 m above the surface) are shown at each grid point. Isotachs are indicated by shading with light shading 5–10 m s^{-1} and medium shading 10–15 m s^{-1}.

value seems too large over the Sahara. In this respect, the GISS global model (Stone *et al.*, 1977) handled the hydrological process over deserts and the simulated 500 mb patterns appear better. It is possible that the treatment of the Sahara and the Asian monsoon had an impact even on the simulation of the troughs over Iceland and western Siberia. (The GFDL climate model and the GFDL global prediction model had reasonable results in this respect.)

At 50 mb (not shown) the predicted pattern looks entirely different from the observed. This is another manifestation of the erroneous intrusion of the midlatitude tropospheric westerlies into the stratosphere, resulting from the poor vertical resolution of the prediction model, as was mentioned in the discussion of Fig. 2.

4. Transient circulation features

a. An example of forecast maps

Fig. 6 is an example of forecasts with this model at days 2 and 4, starting at 1200 GMT 2 July 1970. The case was selected randomly for display; it is neither the best nor worst among the 12 July cases. The development of a low on day 2 in the eastern part was successfully simulated, but the cutoff low on the 500 mb map was not well reproduced. On day 4 the trough at the 500 mb level in the eastern United States was predicted but the position of the predicted trough was somewhat westward relative to the observation. This phase lag is even clearer on the sea level pressure map.

Another example of the forecast map over the entire Northern Hemisphere is shown later in Fig. 23.

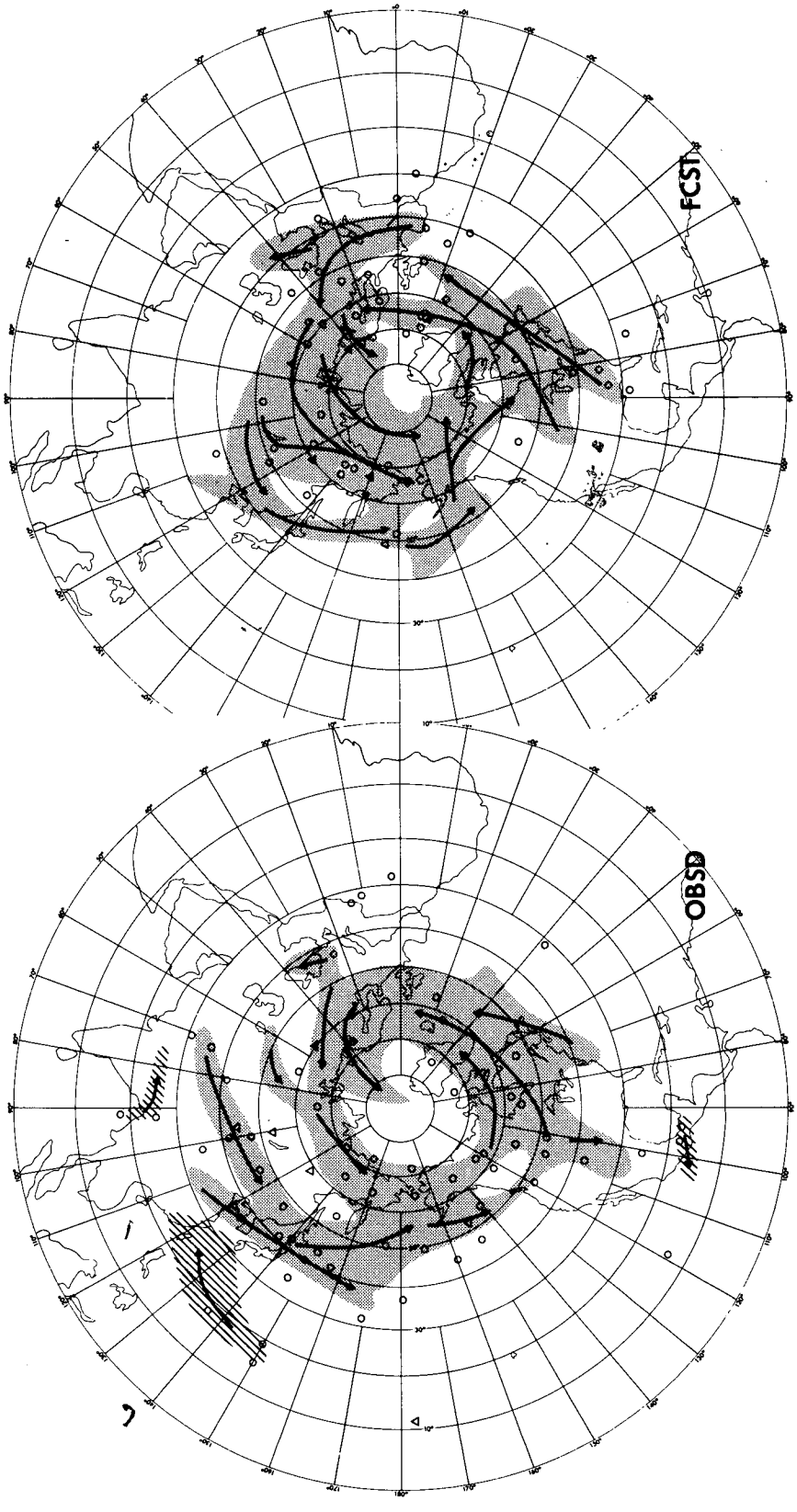

FIG. 7. Observed and predicted cyclone tracks (shaded area), locations of cyclone generation (circles), and locations of cyclone splitting (triangles) on 1000 mb height maps during the period of the 12 July cases. See text for the explanation of the shaded area.

b. Cyclone tracks

Klein (1957) and Petterssen (1956) made comprehensive studies of cyclone paths and locations of formation. A similar study was also conducted only for the cases we treated. The accumulated cyclone tracks of the prediction and the observation are shown in Fig. 7. In order to construct this figure, individual cyclones tracked every day on 1000 mb geopotential maps for both observation and prognosis were plotted, and then the areas of high-density cyclone tracks were shaded. The mean tracks were indicated by arrows.

The cyclone paths have a general tendency to run from west to east and to be directed northward, forming spiral shapes around the arctic zone. There are two major tracks in all seasons; one (Atlantic–Arctic track) runs from North America to Scandinavia or even to the middle of Siberia, and the other (Pacific track) from east of the Asian Continent or from eastern Siberia to the west coast of North America.

Compared with the January case, the most outstanding feature in July is that the principal tracks are shifted poleward by ~10° latitude (Klein, 1957; Reitan, 1974). In more detail, the July case is characterized by the Pacific track ending at the Bering Sea or Alaska rather than reaching the west coast of Canada or the United States as in January, and also characterized by the Atlantic–Arctic track containing a large number of cyclones over the middle of Scandinavia and extending even to northern middle Siberia rather than running at northern Scandinavia and ending at Novaya Zemlya as in January. In the July case, the tracks of the Mediterranean

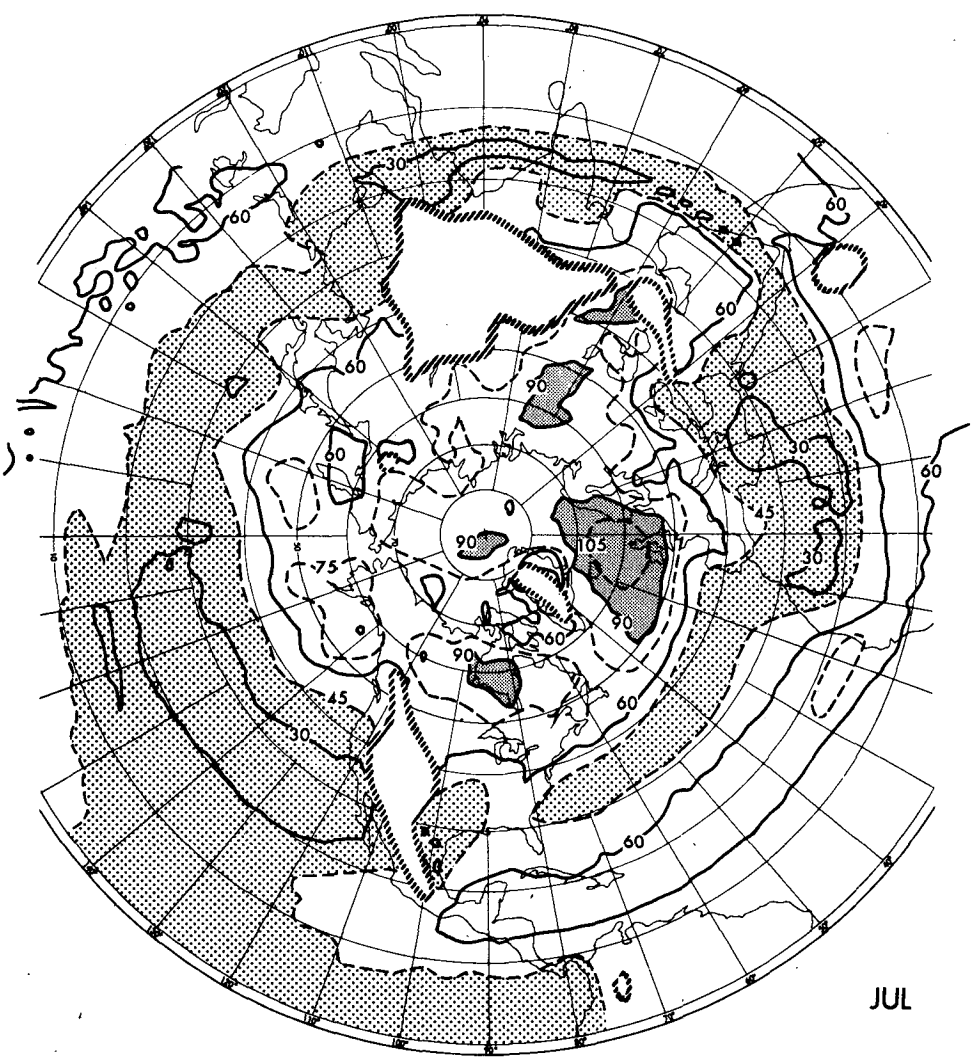

FIG. 8. The rms height error $[E(\delta z)^2]^{1/2}$ for the 1000 mb level. The contour interval including solid and dashed lines is 15 m. The areas in which the error is larger than 90 m are shaded, and the areas in which the error is less than 45 m are stippled.

cyclones are less than in January or, particularly, in April. It is also typical in July that there are more cyclone paths over eastern Siberia and China.

The correspondence between prediction and observation is somewhat poorer in July than in January. There is reasonable agreement between forecast and observation in the tracks over North America, the North Atlantic, the North Pacific and central Siberia. However, the movement of cyclones over China is very different from the observation [see also Kasahara (1977) for the result of the NCAR model.] Reed and Kunkel (1960) mentioned that cyclones develop along the northern shore of Siberia, Alaska and Canada in summer, and that these cyclones frequently invade the central Arctic. Fig. 7 agrees with this description.

In the tropical region, there are cyclone displacements directed clockwise in the observation map. They correspond to the paths of easterly waves which travel westward in trade winds in the tropical Pacific, central Africa, Caribbean Sea and the east Asian monsoon area. However, they are almost entirely missing in the prediction, partially due to the effect of the equatorial wall.

Newton (1956) discussed the lee cyclogenesis over the central eastern slopes of the Rocky Mountains. In our prediction period this phenomenon occurred quite often and was not well predicted. For the present numerical model, one of the most difficult problems is simulating the rapid development of cyclones in the lee of mountains and the subsequent development of cutoff lows [or at the side of mountains, Genoa cyclones, for example (see, Egger, 1972; Mesinger, 1977; Bleck, 1977)].

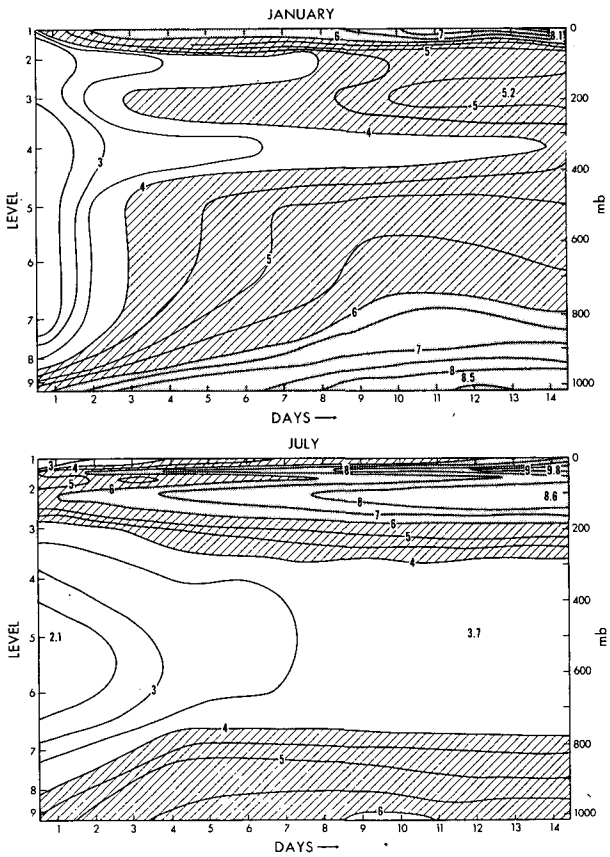

FIG. 9. Time evolution of the rms temperature error (°C) as a function of height. January (above) and July (below). The ordinate is scaled in equal pressure intervals (mb) at the right, and scaled by the nine levels at the left.

c. *Error in geopotential height*

Fig. 8 is the rms error of 1000 mb height defined by $[E(\delta z)^2]^{1/2}$, where E is the ensemble mean of 12 cases. As expected, substantial errors are located mostly in relatively higher latitudes, compared with those of January.

The magnitude of the July rms error is smaller than the January error; the maximum in July is 105 m, whereas it is 180 m in January. The largest errors occur in four regions, i.e., the Iceland-England-Norway area, near the Caspian Sea, northern Canada and the Kamchatka area.

If one compares this map with the rms geopotential field (not error but natural variance) produced by Blackmon (1976), there is a striking resemblance, although his map is for 500 mb and his period is from 15 May to 14 September. This correspondence implies that the geographical locations of these errors may not necessarily be special for this particular model, but they are rather intrinsic in the sense that they were produced by inherited instability of the atmosphere in the respective months.

According to the study of Blackmon, the rms field is largely contributed by a slowly varying part (period >10 days) of spatially medium-scale waves, and yet the contribution from waves of periodicity 4–10 days is not negligible either. In contrast to the winter case, the activities of not only the large-scale slowly varying part but also the small-scale (cyclone) part of atmospheric disturbances affect significantly the rms errors in the summer case.

In Fig. 8 other large rms errors appear in the subtropics, i.e., 10°N over Africa, 20°N in the Atlantic and ~5–10°N in the western Pacific.

d. *Temperature error development*

Fig. 9 is the growth with time of the rms temperature error $[E(\delta T)^2]^{1/2}$, as a function of vertical level, based on six cases each for January and July. The January pattern in Fig. 9 is the same as that in Part I, except that the pressure coordinate was taken for the ordinate in this paper.

The errors seem to start near the surface and tropopause levels, develop quickly in the lower troposphere (~4 days) and somewhat slowly at the

tropopause level (~9 days), and approach their asymptotic value in two (or three) weeks. In July the error growth appears slow near the surface (due to the less intense baroclinicity in summer) but is more rapid at the tropopause. In both January and July cases the minimum error level is located in the middle or upper troposphere.

An equivalent diagram for the winter was shown by Druyan *et al.* (1975) with respect to the GISS model. The result was very similar to that of GFDL even quantitatively, indicating that this quantity is relatively insensitive to models and statistical procedures. Druyan *et al.* also computed the rms error for persistence and concluded that "the model forecast is definitely superior to persistence only during the first few days and it is somewhat superior during the second week."

In general, the error undergoes the transitional period in the first 3 days, say, and grows toward the asymptotic level between the 10th and 20th day [see Smagorinsky (1969) for the extended range]. In the short-term forecasts the initial condition affects the solutions significantly, and the model's capability in simulation of the phase speed of wave disturbances and in prediction of the vorticity distribution is of the utmost importance. Beyond the third day, the physics near the surface starts to exert an essential role and the effect appears to be transmitted to the upper levels.

During the period 10–20 days, the rms error reaches the asymptote; the level is determined by the natural variance plus the model's variance relative to the climate mean. This vertical distribution of errors appears to follow linear baroclinic instability theory (see Kuo, 1952), although the theory treats perturbation amplitudes and we are referring to errors. Note that this feature is also consistent with the vertical profile of the temperature variance obtained in a general circulation model (Hayashi and Golder, 1977). In other words, these errors were caused mostly by the nature of the atmospheric dynamics rather than by the model's bias or the initial data error. The temperature error has maxima near the surface and tropopause, whereas the error of zonal wind, for example, has maximum in the upper troposphere, as shown by Druyan *et al.* (1975).

5. Verification scores

The foregoing sections concern the model's climatology or, exactly speaking, the 10-day averages. We will next proceed to the model's forecast of the day-to-day variations during the two-week period.

The performance of the prediction was examined by a number of skill scores. The measures of skill used in this paper are the standard deviation of height error, the correlation coefficient between the observed and the predicted height anomaly, and the correlation coefficient between the observed and predicted Laplacian of height anomaly (Part I). Another measure is the $S1$ score (Teweles and Wobus, 1954). Two verification domains will be used below, i.e., the Northern Hemisphere and the contiguous United States. The Northern Hemisphere which we refer to in this paper was confined to that north of 20°N because of the limitation in the NMC analysis, and possibly because of contamination in the forecast south of 20°N caused by the equatorial wall.

Fig. 10 shows the growth with time of the standard deviation of geopotential errors for 1000, 500 and 50 mb levels over the verification domain of the Northern Hemisphere. The thick curves in the middle of the shaded areas are the ensemble means for 12 cases, and the dashed curves are the mean persistence for the same samples.

In the July case, the mean curve at 500 mb is lower than the persistence curve for the entire two weeks. The persistence is shown only for a reference. The fact that the curve lies below persistence does not necessarily imply that positive skill is proven. The curve for 1000 mb is always above persistence in the July case, and the skill for 50 mb deteriorates quickly and the standard deviation of geopotential errors is far above persistence.

In this paper, the rms value of climatology (or the monthly normal which was used in Part I) was not shown, since there is an increasing opinion that the comparison of the errors of the monthly normal is misleading rather than elucidating (though the climate mean is simply an additional reference). As Leith (1974) has demonstrated, the rms error for any forecast pattern can be reduced below the level of the errors of the monthly normal by manipulation of the climatological pattern in the context of a regression forecast. The rms error is a meaningful assessment measure if various forecast results in examination are produced under exactly the same conditions.

The correlations for anomalies $Z - Z_n$ of the 1000, 500 and 50 mb heights are shown in Fig. 11, the verification domain being the Northern Hemisphere. The mean values of correlations for 1000 and 500 mb are positive for two weeks, although the correlation curves cross the respective persistence curves at day 8. On the other hand, the correlation at 50 mb is considerably lower than the persistence; the July stratosphere was indeed poorly simulated.

Fig. 12 is the correlation of $\nabla^2(Z - Z_n)$ for 500 mb over the Northern Hemisphere. The value is not high compared with the correlations for the height itself; it drops rapidly and reaches close to zero at about day 5. This correlation in July is slightly lower than that in January, apparently reflecting the difficulty of vorticity forecast in the summertime.

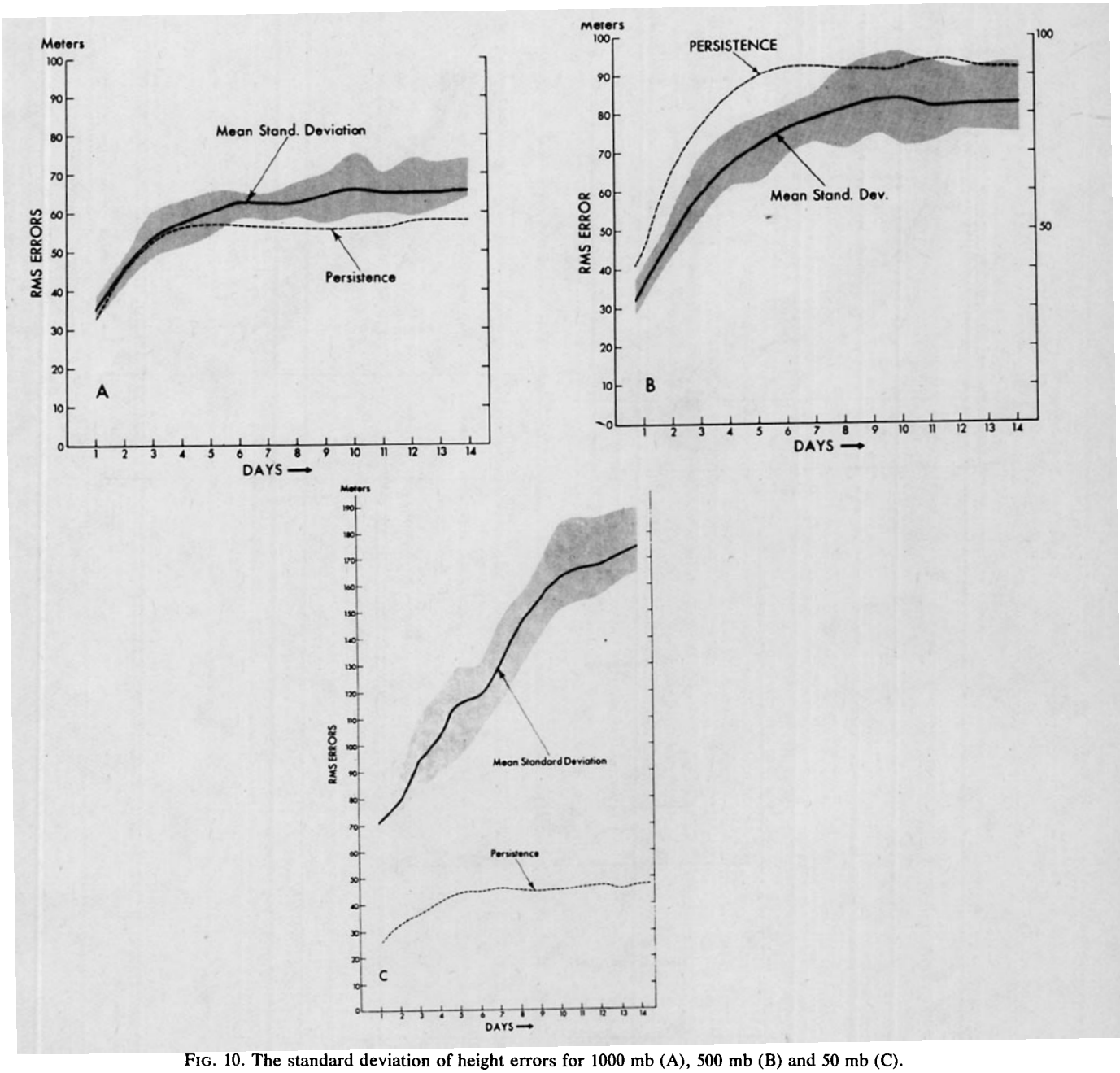

FIG. 10. The standard deviation of height errors for 1000 mb (A), 500 mb (B) and 50 mb (C).

The $S1$ score treats the horizontal gradient of height. Since this score has been used for many years at NMC, we also calculated it (Fig. 13). The verification domains are the contiguous United States and the Northern Hemisphere. Although the sample number for the verification over the United States may not be sufficient, the hemispheric score may be acceptable.

It appears from the 500 mb score that 1) the $S1$ scores reached their asymptotes at about 8–10 days and that 2) the $S1$ scores consistently were better than the persistence scores until the 10th day. The 1000 mb score (not shown) indicates that the $S1$ scores reached persistence levels at about 4–5 days.

Comparing the values of correlation coefficients for July and January (Fig. 14), one may find that the July forecasts are poorer in the first 5 days than the January forecasts, but beyond the 6th day the forecast skill for July stays slightly above that for January at 1000 and 500 mb.

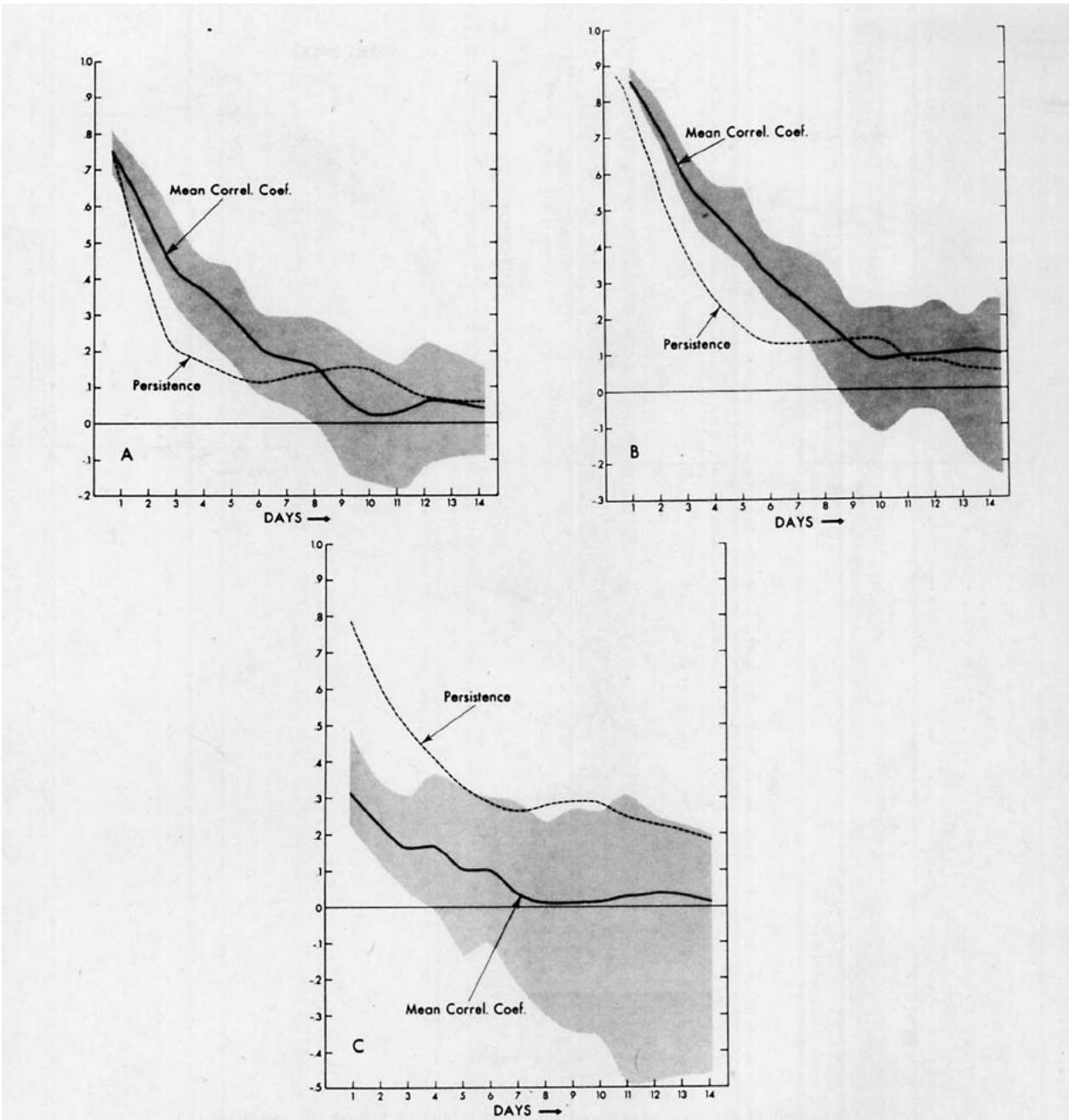

FIG. 11. The correlation coefficients for height anomalies for 1000 mb (A), 500 mb (B) and 50 mb (C).

6. Spectral performance

The geopotential heights for a zonal belt were decomposed into Fourier series, i.e.,

$$Z(\lambda) = \sum_{k=1}^{n} A_k \sin 2\pi k\lambda + \sum_{k=0}^{n} B_k \cos 2\pi k\lambda,$$

where λ is the longitude. Fig. 15 compares the 12 cases of the observed and predicted spectra of geopotential height, $A_k^2 + B_k^2$, in a zonal belt.

In Part I, we took the latitudinal belt between 35 and 45°N. In July, it appears appropriate to take the belt between 45 and 55°N, because the belt for 35–45°N in July is not the region of maximum intensity of disturbances in the westerlies. Klein's (1957) maps indicate that the cyclogeneses are most intense at 35–45°N for January and at 45–55°N for July.

It is interesting to note that the amplitudes at 1000 mb are large at the lowest wavenumber regime compared with those at 500 mb. This characteristic is just opposite to that in the winter. The fact is first

due to the predominance of the two anticyclones in the vast oceanic areas in July, and second, the baroclinicity is less in July and accordingly the disturbances at 500 mb are less. It is also striking that the 1000 mb amplitude in prediction is much larger than in the observed for the wavenumber range from 2 to 21.

a. Verification of the geopotential height for various scales

The correlations between predicted and observed geopotential were calculated for each of four spectral bands, i.e., wavenumbers, 1–2, 3–5, 6–10 and 11–18 in the 45–55° belt. The correlations are obtained for anomalies of height (labeled Anomaly in Figs. 16–18), for the total height (labeled Total), and for persistence of the initial anomaly (labeled Persist). These scores have been averaged over the 12 cases. Numbers are plotted along the abscissa in the figures; for example, in waves 3–5 in Fig. 17, day 7 is the time at which the correlation for the anomaly becomes zero.

Different from the January case, the correlations for the waves 1–2 stay high until day 12, implying that the planetary waves were relatively better predicted. This may be the reason why the July case continues to maintain a high overall score as was shown in Figs. 11 and 14. The reason why the planetary waves are better simulated in July than in January is not certain. One speculation is that the planetary wave prediction becomes difficult if the orographic effect is included, and that in the January case the main westerly flow runs at 35–45°N where there are more high mountain barriers than at 45–55°N.

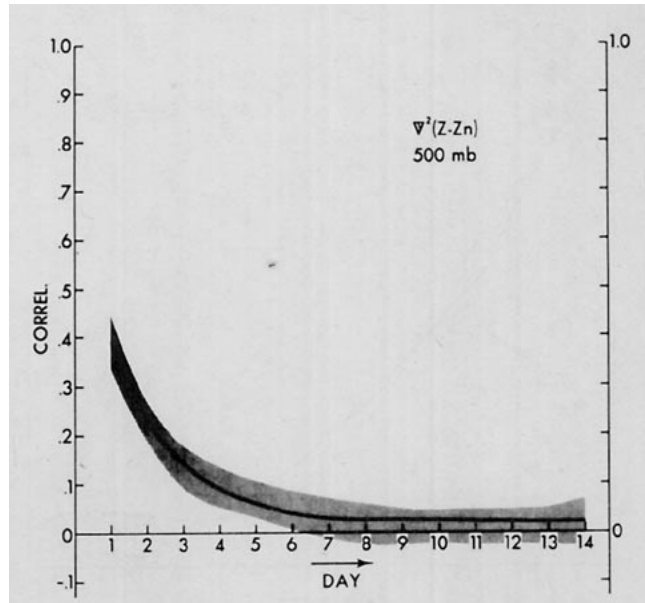

FIG. 12. The correlation coefficients for the Laplacian of 500 mb height anomalies.

In this paper, we took a one-dimensional spectrum. Baer (1972) advocated a two-dimensional spectrum in terms of n in spherical harmonic functions, $Y_n^m = P_n^m e^{im\lambda}$, where n is the degree and m the rank (zonal wavenumber), and P_n^m is an associated Legendre function. However, we did not follow his suggestion in this paper, mainly because we wanted to compare the results with Part I, and partly because more readers are familiar with the one-dimensional representation in linear perturbation theories. Concerning the classification of the wavenumber,

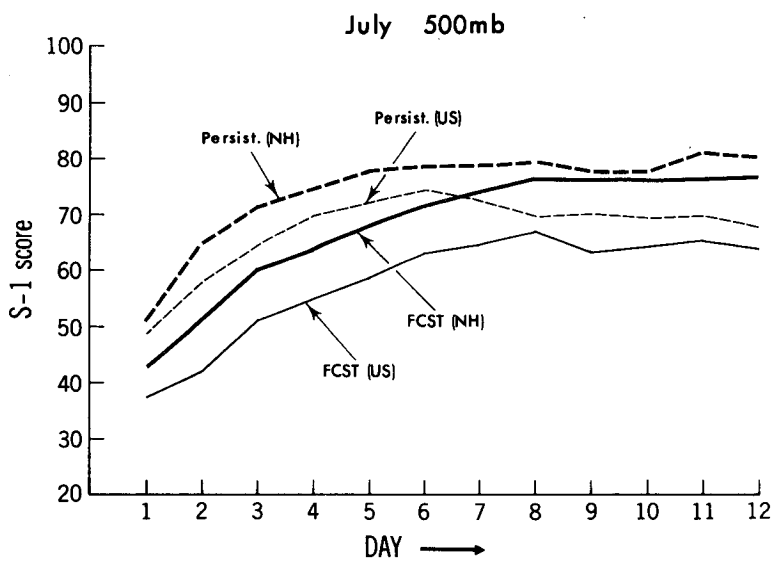

FIG. 13. The $S1$ scores of 500 mb heights over the Northern Hemisphere (NH) and the United States (US). The solid curves are for the forecasts and the dashed curves for the persistences.

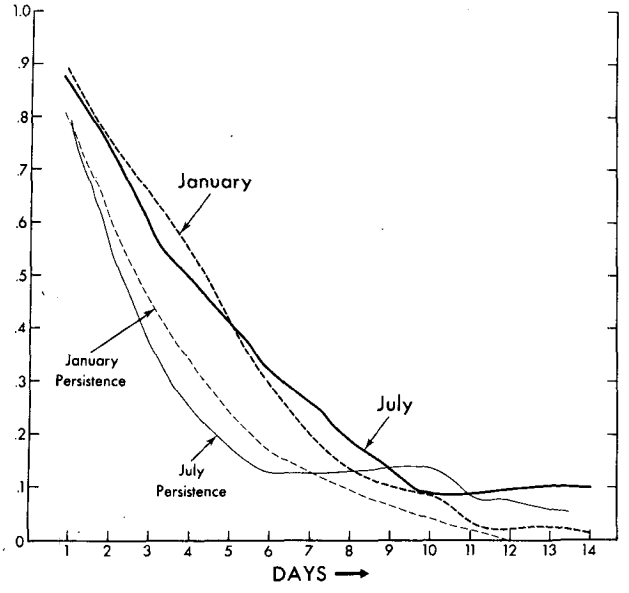

FIG. 14. Comparison of the correlation coefficients between January and July for 500 mb.

JOC WGNE (Joint Organizing Committee/Working Group on Numerical Experimentation) of GARP suggested the use of three zonal wavenumber ranges —large scale (m = 1–3), intermediate scale (m = 4–9) and small scale ($m \gtrsim 10$). Arpe *et al.* (1976) and Baumhefner and Downey (1976) used this classification. Perhaps three classifications may be simple and sufficient.

7. Critique on the model

a. Speculated deficiencies of the model

Part I included several critical remarks on the 1967 version of the GFDL model, and possible future improvements were mentioned. In the following seven years, a number of studies related to this subject have been conducted in various places. In particular, the intercomparison between models within the context of the short-range or extended-range forecasts have been undertaken, using the identical initial data set in the respective studies (Baumhefner and Downey, 1976, 1978; Houghton and Irvine, 1976; Baumhefner, 1976; Arpe *et al.*, 1976; Carson, 1978; Hembree, 1977; Phillips, 1978). Guided by these studies and partly based on the experiences in our forecast experiment, some of our views on this model have been reconfirmed and others have been appreciably altered.

The current view on the deficiencies and accordingly the need for revision of this particular model are listed below.

1) SPACE RESOLUTION

Further refinement of horizontal resolution is required (see, e.g., Miyakoda *et al.*, 1971; Williamson, 1978). The grid distance in the 1967 version model is $2\Delta S$ = 540 km at 60°N between two geopotential heights for the calculation of geostrophic wind and for horizontal advection; this resolution does not appear to be small enough for the 10-day forecasts.

With the low spatial resolution model of the 1967 version, the calculated flow pattern tends to include small-scale irregularities as time increases. The vorticity patterns start to be shredded, and the "spaghetti" distribution shows up (Platzman, 1961), although the computational stability is still maintained (see Miyakoda *et al.*, 1971; Umscheid and Bannon, 1977). The shredded pattern will start to show up on day 7 with the N = 40 resolution of grid on the stereographic projection map in the 1967 version model, while the same feature did not appear before day 14 in the N = 80 resolution model.

Williamson (1978) concluded, however, that "the improvement in the amplitude of the largest scales (wavenumber 1–3) with the finer resolution can be attributed to the accompanying decreased diffusion rather than more accurate approximations". In other words, if there were a highly selective subgrid-scale viscosity formulation which does not affect the planetary-scale solution and yet maintains the computational stability, the high-resolution model would not be needed. Williamson's discussion concerns the 5-day forecasts. In the 10-day range, the decascade effect of energy from the baroclinic-scale wave to the planetary wave in the sense of Fjørtoft (1953) becomes appreciable. For this reason, a higher resolution model beyond N = 40 seems necessary. Furthermore, from the standpoint of rainfall forecasts, the N = 40 resolution is definitely not sufficient.

It was also desired to increase the vertical resolution not only in summer but also in winter. It was found (Miyakoda, 1975) that the higher vertical resolution model produced larger amplitudes of large-scale waves in the midlatitude troposphere in winter. Derome (personal communication) has recently mentioned that a model which has more levels in the stratosphere may produce more intense planetary waves in the winter troposphere, because the taller model can reach stronger westerlies in the deep stratosphere, and as a result, the leakage of wave energy into space is prevented.

2) ENSTROPHY CONSERVING FINITE DIFFERENCE

The notion of enstrophy conservation in finite-difference formulation has been advocated by Arakawa (1966), Sadourny (1975) and Mesinger and Arakawa (1976), although a convincing explanation for the necessity has not been established yet. Perhaps the conservation itself is not the major issue where a stable marching calculation is already guaranteed. But a careful and appropriate treatment of local vorticity in the numerical calculation may be important

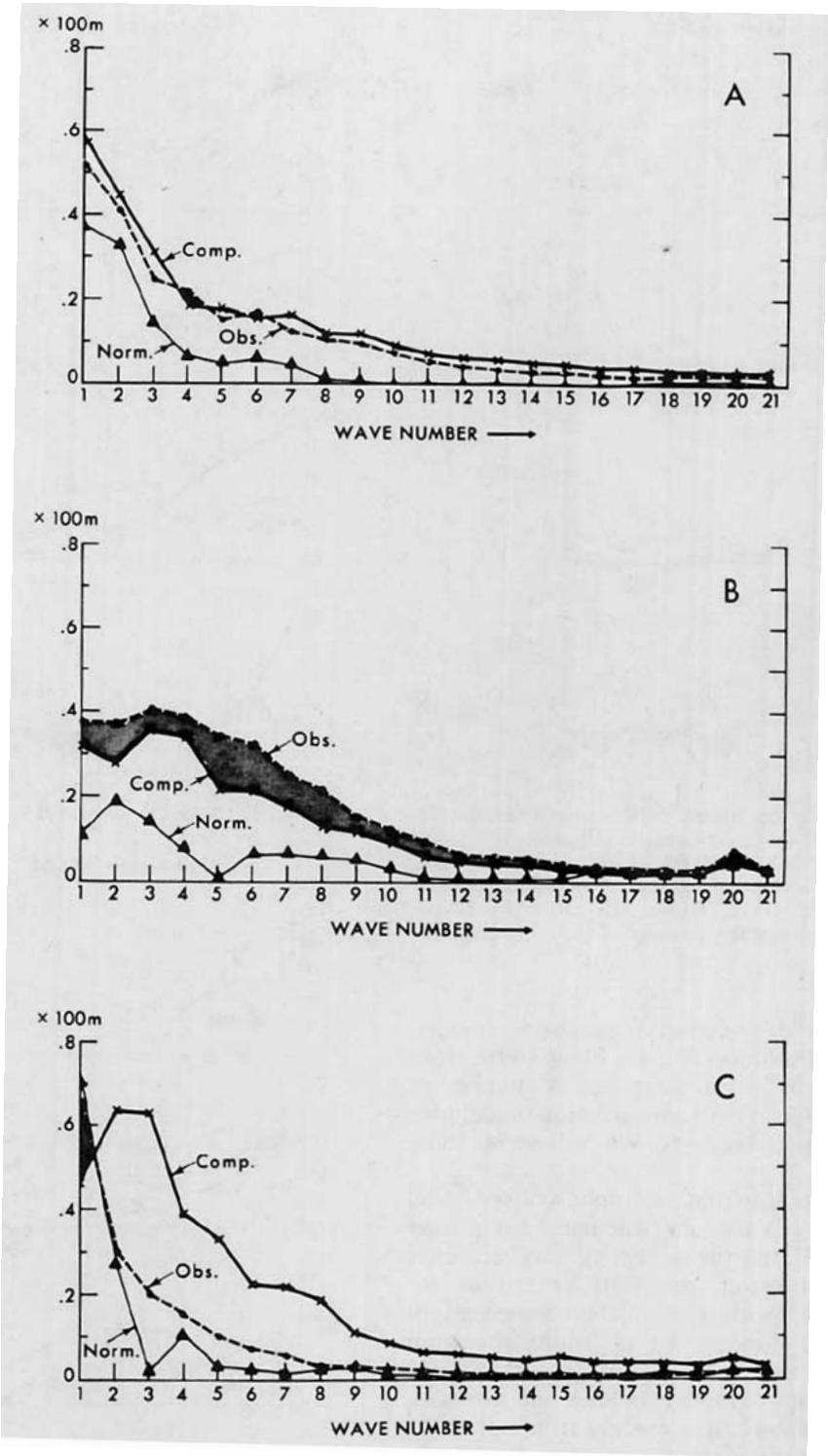

FIG. 15. Spectra of geopotential height for 50 mb (A), 500 mb (B) and 1000 mb (C). Circles indicate observation; crosses, prediction; and triangles, the climatological normal.

for extended-range forecasts, and enstrophy conservation may give a guiding principle for a finite-difference formulation to achieve it.

By deliberate choice, the finite-difference scheme in the 1967 version model was formally intended to conserve kinetic energy, not enstrophy. The recent study in the European Centre (Baede and Hansen, 1977) showed that the enstrophy-conservation grid-point model produced forecasts more similar to those of a spectral model rather than those

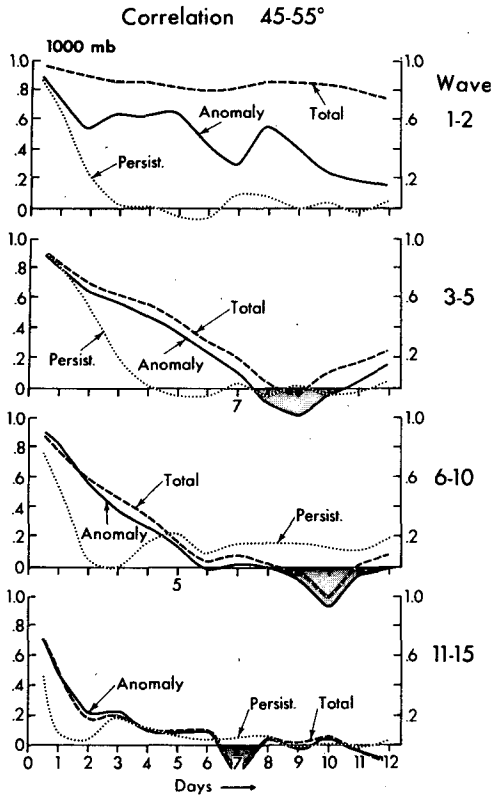

FIG. 16. Correlation coefficients between predicted and observed heights for various spectral bands of geopotential height at 1000 mb for 45–55°N latitude. Total is referred to as the correlation with respect to the total height Z in contrast to the anomaly, $Z - Z_n$, where Z_n is the climatological norm. Persistence is the correlation between the anomaly of the initial time and the observation.

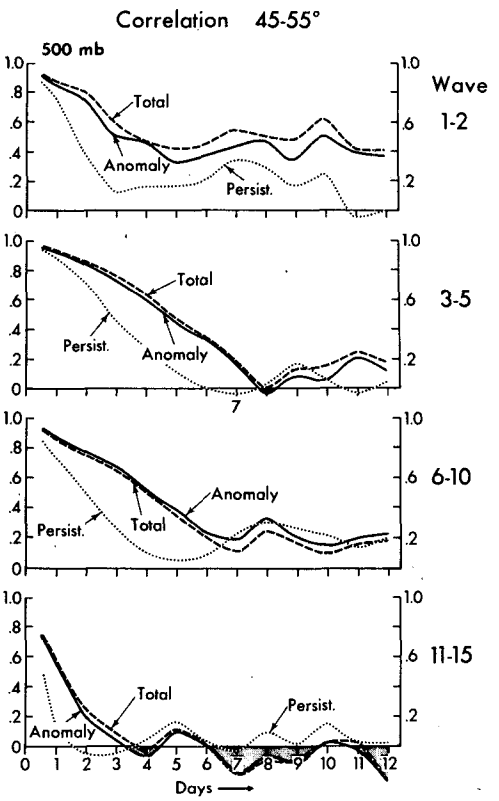

FIG. 17. As in Fig. 16 except for 500 mb level.

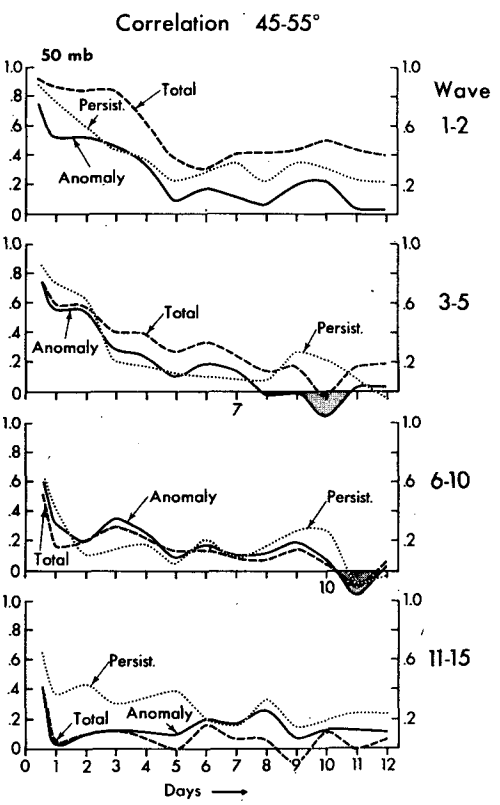

FIG. 18. As in Fig. 16 except for 50 mb level.

of only a kinetic-energy-conserving grid-point model. However, which solution is more likely to be close to the observation is not clear yet. A number of people think the enstrophy-conservation model provides more correct forecasts. We will show some examples later.

There is a possibility that enstrophy-conservation finite differencing is useful particularly for a low-resolution model, and the necessity may decrease with increase of resolution. With regard to enstrophy, Puri and Bourke (personal communication) consider that the slope of the enstrophy spectrum curve in wavenumber space is a useful criterion for evaluating whether a model handles the vorticity calculation adequately. It is evident from a number of experiments that a -3 power spectrum of kinetic energy is approximated by any general circulation model, but a suitable enstrophy spectrum is not readily obtainable. Theoretically, a nondivergent flow with a -3 power spectrum for kinetic energy is supposed to have a -1 power spectrum for enstrophy. However, Gordon (1976) has showed that his three dimensional spectral model produced an

enstrophy spectrum of -1.5 power at midlatitudes instead of a -1 power, implying that spectral resolution may not be sufficient for the vorticity calculation.

3) THE STAGGERED GRID

Arakawa and Lamb (1977; see, also, Mesinger and Arakawa, 1978) argued that the A-lattice which our model uses leads to an erroneous wave dispersion relation and inefficient geostrophic adjustment in the finite-difference solution. A more direct description of the disadvantages of the A-lattice system may be a statement that it enforces a redundant calculation generating multiple-computational modes of solution, which might give an adverse effect rather than an improvement of the solution.

The shredded flow pattern mentioned earlier may be related to the problem above. In other words, the shredded pattern is the consequence of using the A-lattice, but the A-lattice is not the generator of the shredded pattern.

4) THE MOUNTAIN TREATMENT

A proper treatment of pressure gradient terms in the equations of motion in sigma-coordinate is essential to the accurate inclusion of the topographic effect (Mesinger, personal communication; Kasahara, 1977). In this respect, the 1967 version model may not be satisfactory (see Miyakoda, 1973). A finite-difference treatment of the term of adiabatic expansion/contraction ($-\omega\alpha$) in the temperature equation must be consistent with the formulation of the pressure-gradient terms (Corby *et al.*, 1977).

Moreover, Arakawa and Lamb (the following material that replaces Section III-C of their 1977 paper) reported that schemes of potential enstrophy conservation are very effective for accurate inclusion of the effect of the large-scale mountain barrier, and suggested that the deficiency in the simulation of the ultralong waves in conventional models may be rectified. Burridge and Haseler (1977) have already incorporated this feature in the model of the European Centre for Medium-Range Weather Forecasts, and the model was implemented for the test prediction of medium-range weather evolution (see Gauntlett *et al.*, 1977).

5) THE SUBGRID-SCALE VISCOSITY

Smagorinsky's (1963) nonlinear viscosity has been used in our model. We found this viscosity is useful because of the highly scale-selective dissipation particularly compared with the formula $K\nabla^2$. A powerful dissipation for the high-wavenumber flow is required to obtain an overall favorable forecast. Francis (1975) demonstrated that the removal of very small-scale disturbances allows more active general circulation in the model solution, such as high levels of eddy kinetic and potential energies, and Ferrel as well as Hadley cells, which are closer to the observation.

Smagorinsky derived the formulation of his viscosity based on a heuristic assumption: the Reynolds stress is proportional to deformation of flow and the energy spectrum obeys the $-5/3$ law. Interestingly, Lilly (1967), and Deardorff (1973) obtained Smagorinsky's formula from the theory of turbulent closure by discarding many terms, and also found that the coefficient for temperature diffusion is much larger than the coefficient for momentum.

The coefficient varies with the grid size ΔS adopted. As was mentioned earlier, experiences of real-data forecasts are that less influence of the subgrid-scale viscosity on the lower wavenumbers is more desirable. In this view together with the reason of economy, Hoskins, (personal communication) proposed an empirical $K\nabla^4$ viscosity and Williamson (1978) suggested $\nabla^2 K \nabla^2$ viscosity. According to our experiment, $K\nabla^4$ viscosity gives better forecasts than Smagorinsky's nonlinear viscosity (Gordon, personal communication).

6) THE LAND-SEA DRAG AND THERMAL CONTRAST

According to a sensitivity study on surface layer processes (Delsol *et al.*, 1971), the land-sea contrast of drag and thermal diffusion is most influential on the forecast of extended range, compared with other processes such as the Monin-Obukhov process versus the neutral process and the diurnal variability versus the nondiurnal treatment. Garratt (1978) has reviewed the observational data of the drag coefficient, summarizing that the neutral drag coefficient C_{DN} referred to 10 m/height is $C_{DN} \times 10^3 = 10$ over land and $C_{DN} \times 10^3 = 0.75 + 0.067\,V$ over sea, where V is the wind speed (m s^{-1}). Over mountainous areas, the form drag arising from flow over rugged topography is considerable, but the effect is not included in C_{DN} above.

Note that the impact of the differential drag on the large-scale flow is only appreciable on the forecasts beyond 6 days.

7) "MOIST CONVECTIVE ADJUSTMENT"

Miyakoda (1975) made a comparison test by including or excluding some processes in or from a prediction model. The conclusion is that the water vapor effect is very important in improving the medium-range forecast. Heat released by condensation activated the flow pattern and the forecast score was thereby improved over the forecast without water vapor processes.

For the parameterization of ensemble cumulus convection, the moist convective adjustment scheme has been incorporated in the 1967 version model.

The scheme is a simple and reasonably good parameterization. Yet the "shocking" generated by the scheme seems harmful for the meteorologically significant part of numerical solutions, and the effect may be aggravated by use of the nonstaggered grid. Hollingsworth (1977) pointed out that the scheme of moist convective adjustment produces a seemingly spurious secondary frontal circulation. The shocking (i.e., the generation of gravity waves) may be alleviated in several ways, such as non-instantaneous removal of the instability.

However, there is yet another aspect—the depth of the convection layer or the vertical distribution of heating and momentum. The heating in the "moist convective adjustment" is weighted in the lower layer between 900 and 500 mb more than that in the cumulus convection scheme by Arakawa and Schubert (1974). In other words, the latter produces a deeper penetrative convection (Miyakoda and Sirutis, 1977). Recently, Hollingsworth (personal communication) has investigated this point, comparing the moist convective adjustment with Kuo's scheme, and concluded that the former produced the shallower penetrative convection. Hollingsworth then suggested that this difference leads to a large impact on the baroclinic instability in the middle latitudes.

8) The land evaporation

Because of the crude specification of soil moisture, an excessively erroneous evaporation is taking place in the present model. This problem will be discussed separately in the next subsection.

9) Other factors

The replacement of dry convective adjustment by an appropriate vertical diffusion process may be desirable, simply because the former is too crude (Miyakoda and Sirutis, 1977). The transfer process in the planetary boundary layer could be improved, although a major impact would occur in the tropics. The removal of the equatorial wall is required for

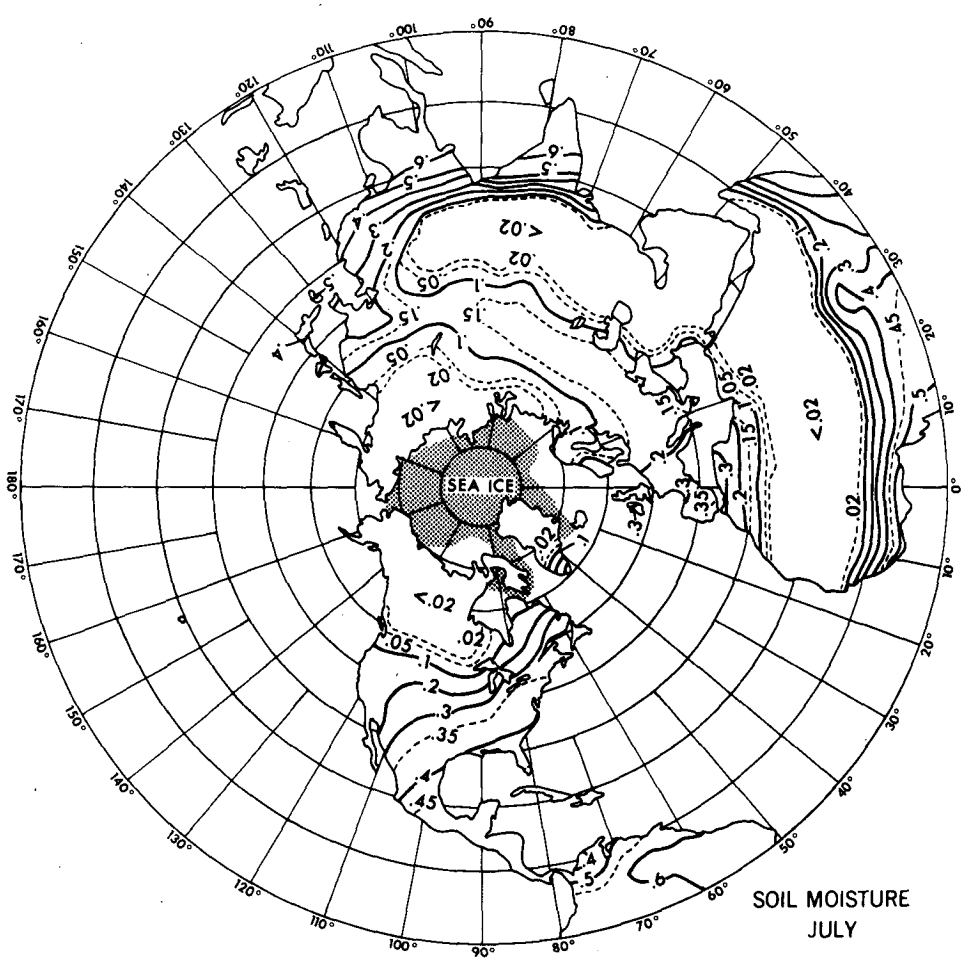

FIG. 19. The availability of soil moisture, w/w_c, used in the extra experiments. The sea-ice area is also shown.

TABLE. 2. Specified relation between rainfall and availability of soil moisture.

Rainfall [cm/(6 month)$^{-1}$]									
$\gamma_w = w/w_c$									
5	10	15	20	25	30	35	40	45	50
0	0	0	0.065	0.130	0.190	0.245	0.291	0.333	0.368
55	60	65	70	75	80	85	90	95	100
0.402	0.432	0.461	0.487	0.507	0.522	0.538	0.554	0.569	0.580
105	110	115	120	125	130	135	140	145	150
0.590	0.600	0.605	0.610	0.615	0.617	0.619	0.620	0.620	0.620

the forecast beyond 8 days. This is particularly important for the summer forecast.

Leith (1978) reviewed the current development of weather prediction and presented his outlook: a stage will be reached where the remaining difficulties arise from a large number of small effects, but the present strategy will identify some medium-sized effects and lead to their correction. The deficiencies mentioned above in this paper may constitute some of the medium-sized effects.

b. *Soil moisture sensitivity*

We made a test on this problem for three cases of 12-day forecasts, using both the control model (1967 version) and a model of the modified soil moisture. The soil moisture w is involved in the estimation of evaporation E_s at the surface, i.e.,

$$E_s = \frac{w}{w_c} E_{\text{pot}},$$

$$E_{\text{pot}} = C_D |\mathbf{V}| [q_{\text{sat}}(T_s) - q_9],$$

where w_c is the field capacity of soil moisture, $\gamma_w = w/w_c$ is the availability of soil moisture, E_{pot} the potential evaporation, q the mixing ratio of water vapor to the dry air, q_9 the mixing ratio at the lowest level of the models (level 9), T_s the surface temperature, $q_{\text{sat}}(T_s)$ the saturation moisture at T_s, C_D the coefficient for moisture flux at the surface, which is equal to the drag coefficient, and $|\mathbf{V}|$ the intensity of wind at level 9.

In the control model, γ_w was set to 1.0 over sea and 0.5 everywhere over land. On the other hand, in the second model, γ_w was 1.0 over sea, whereas γ_w over land was specified as in Fig. 19. These values

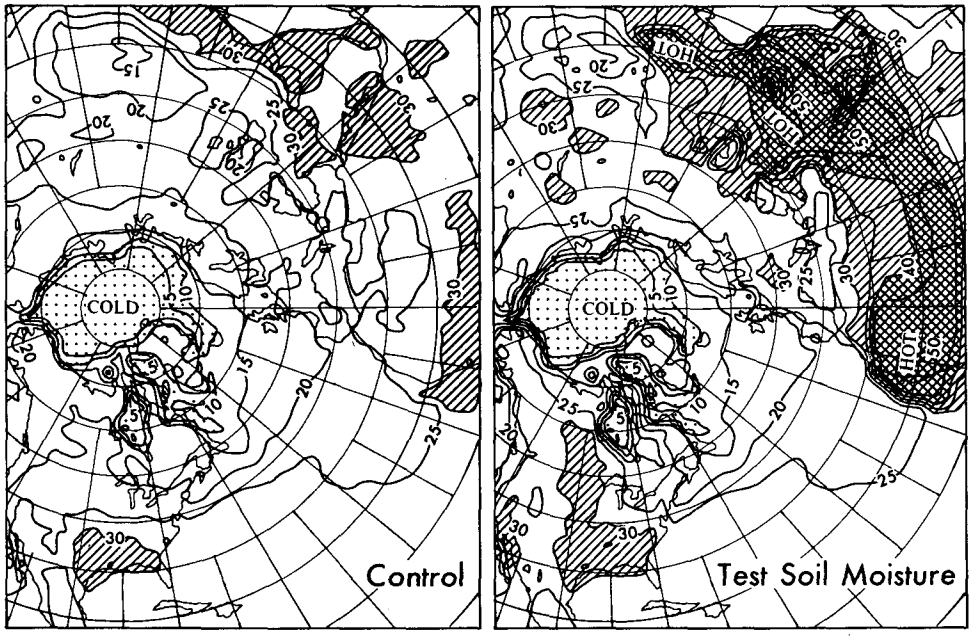

FIG. 20. The 10-day averages (days 2–12) of surface temperature (°C) for the control model (left) and the modified soil moisture model (right).

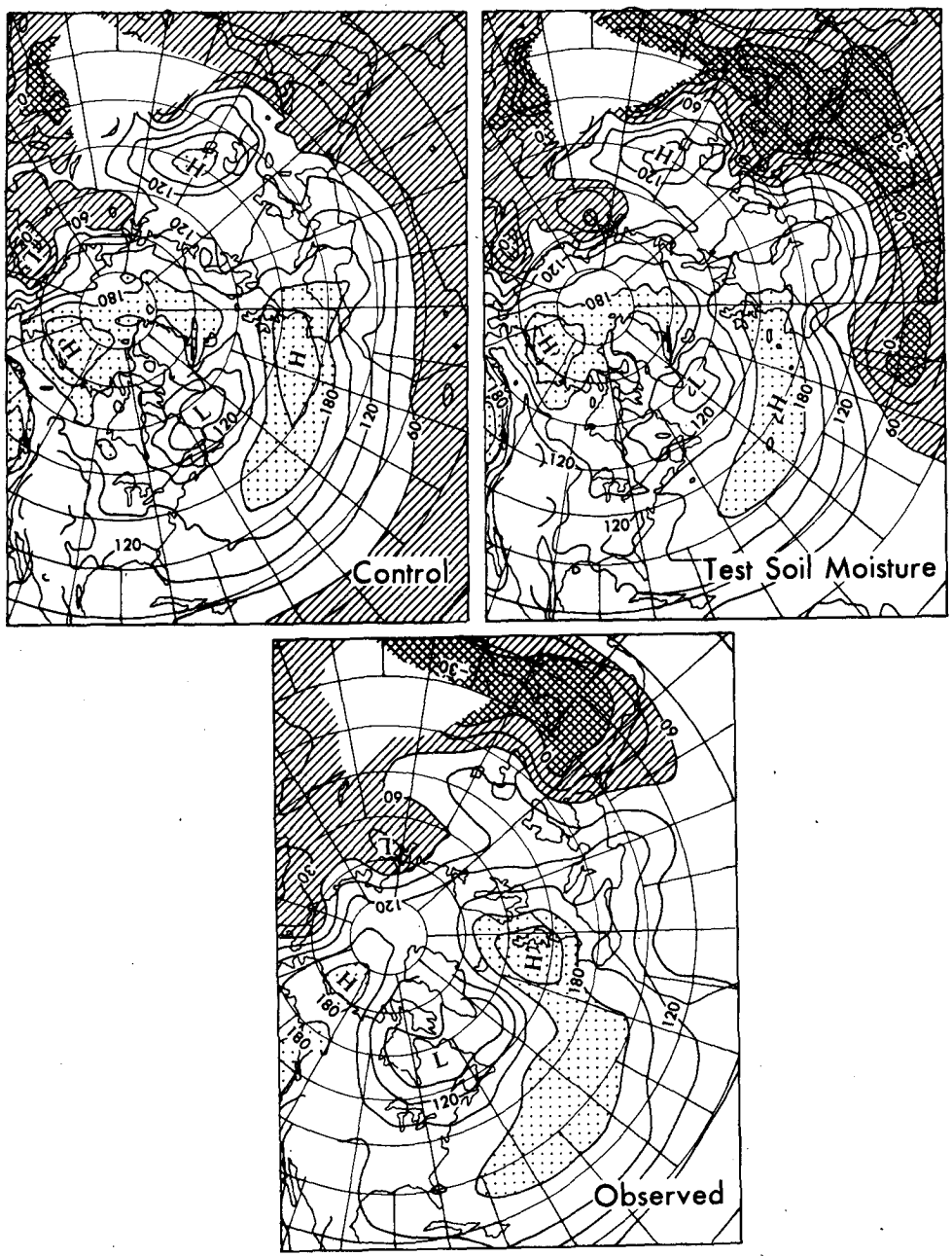

FIG. 21. The 10-day averages (days 2–12) of 1000 mb geopotential height (m) for the control model, the modified soil moisture model, and the observation.

were fixed with time in this experiment, though in the general circulation model, w is often predicted using the equation of soil moisture budget (Manabe, 1969). According to Manabe (personal communication), the adjustment of soil moisture is very slow, say, four months of relaxation time; thus the initial condition for w dominates in two-week forecasts. The values in Fig. 19 were determined from the climatological records of rainfall for July plus the preceding five months (similar to Saltzman, 1967). The empirical relation between the rainfall for six months and w/w_c used in this experiment is given in Table 2. This table differs considerably from that of Saltzman; the values he proposed are very large. Note that, as Priestley and Taylor (1972) showed, γ_w has a good relation with $E - P$, the accumulated actual (not potential) evaporation minus precipitation rather than only the precipitation.

The results for surface temperature and the geopotential heights at 1000 and 500 mb for the 10-day

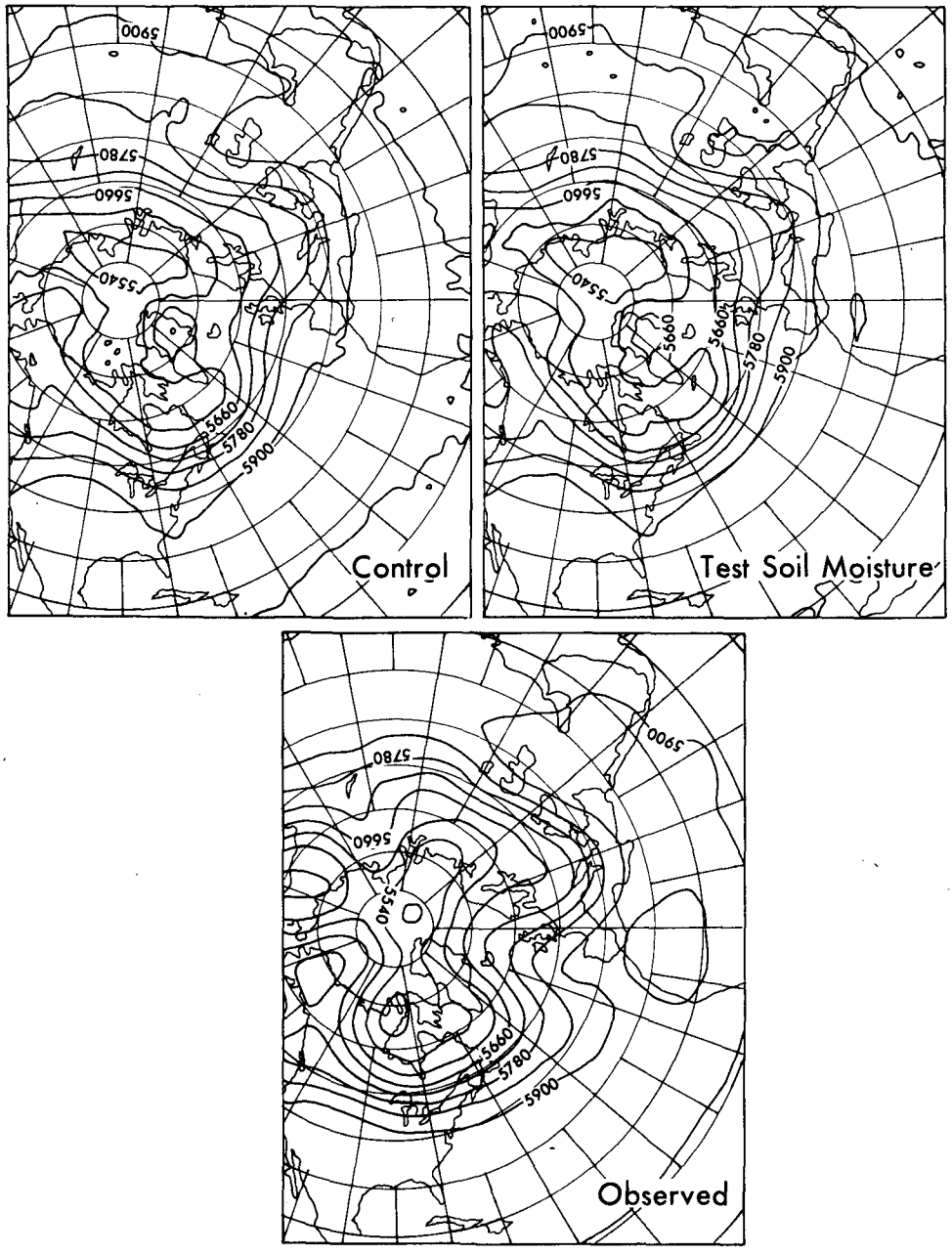

FIG. 22. As in Fig. 21 except for 500 mb geopotential height.

average from 2 to 12 days are shown in Figs. 20, 21 and 22. As was pointed out by Walker and Rowntree (1977), the soil moisture affects the radiation balance at the ground surface through the evaporation and the effect appears to be appreciable not only in the long-period simulation of circulation but even in the 2–3 day forecast. Note that the effect of soil moisture on albedo was not considered here. According to Walker and Rowntree, the warming due to the dry surface was confined below 500 mb, and the cooling resulting from the lack of cumulus convection was as an indirect effect. Fig. 20 shows that the surface temperature has increased by 20°C over the Sahara desert in our case, which is the same as Walker and Rowntree reported. In Fig. 21, the systematic bias of 1000 mb geopotential height in Turkestan appears to be removed, and the lows have been well-established over the Sahara, Arabian and Gobi deserts by the modified soil moisture, though the effect is excessive compared with observation. In the 500 mb maps, highs have been developed at the western part of Africa associated with the

Sahara desert, and the trough over the central U.S.S.R. has been deepened by the new model. It is also important to note that the midlatitude westerlies no longer extend into the tropics.

c. *Numerical approximation comparison*

In the following, in order to clarify the relative capability of the 1967 version model, a comparison of this model with a recently constructed model, i.e., a spectral model, will be presented. It may be interesting to see how a model which is free from some of the above deficiencies performs in short-range and medium-range forecasts.

The spectral transform model was constructed by Gordon and Stern (1974) as a general circulation model based on Bourke's (1972) barotropic model, which uses the spherical harmonic functions as well as the transform grid. Therefore, this model is endowed with the characteristics of enstrophy conservation for two-dimensional terms and of precise estimation of lateral pressure and geopotential gradient terms in the equations of motion (however, the temperature in front of the term $\nabla \ln p_s$, where p_s is the surface pressure, is free to be specified in the vertical). The space resolution in the spectral model is "R30L9", which means that the spectral representation is truncated in rhomboidal fashion of order 30 and that there are nine vertical levels. The rhomboidal truncation 30 means that $M = J = 30$ for $|m| < J$ and $n \leq |m| + J$ for Y_n^m, i.e., the same wavenumbers are contained both for the zonal and meridional directions. The grid numbers at the so-called Gaussian latitudes between pole and equator is $N = 40$; this grid size corresponds to ~242 km. The physics in the spectral model are almost comparable to those in the 1967 version model except that the soil moisture has been improved and the land-sea drag contrast is included.

An example of the predicted geopotential height maps in both models is given in Fig. 23. The initial time is 1200 GMT 16 July 1968. It appears that the spectral model performs reasonably well, particularly at day 8, and seems more skillful than the finite-difference model, although the difference is not large. The averaged skill scores for three cases also are shown in Table 3, where the initial times for the additional cases are 3 July 1966 and 19 July 1969, both for 1200 GMT. The rms error of Z (geopotential height), the correlation coefficients for the height anomaly, and the correlation coefficients of the Laplacian of height anomalies, $\nabla^2(Z - Z_n)$, are shown for the hemisphere poleward of 20°N; they are slightly, but consistently, better in the spectral model than in the 1967 version finite-difference model. On the other hand, the $S1$ score over the United States is worse in the spectral model. It may be interesting to note that the performance of the spectral model is particularly good in the score of $\nabla^2(Z - Z_n)$. This is not inconsistent to the expectation that the spectral model supposedly handles the vorticity calculation better. Previously, Gordon (1976) had made a preliminary comparison of a spectral model with a global finite-difference model ($N = 48$) for one case of March 1965. Also, the rms error of 500 mb geopotential in that test was measurably lower in the spectral model up to the tenth day. Simmons and Hoskins (1975) summarized their comparison experiments using a somewhat idealized initial condition, as that a spectral model gives a more accurate representation of amplitudes and phases in a growing wave than does a finite-difference model, but smaller scale changes such as those of frontal structure are resolved better by a finite-difference model. Baede and Hansen (1977) mentioned that in comparative 10-day forecasts with the spectral and grid-point models each with judicious space resolution there is little to choose between the two models, though anomaly correlation coefficients suggests a slightly better performance of the grid-point model. Baumhefner and Downey (1978) concluded from their study of model-intercomparison that a spectral model (Canada) has good forecast skill in large- and medium-scale baroclinic disturbances. However, they also stated that the GISS finite-difference model is more capable of minimizing the error associated with planetary-wave features than the Canadian spectral model (the GISS model uses the Arakawa finite-difference scheme, i.e., quasi-enstrophy conservation using the B-lattice).

8. Conclusions

Application of the GFDL 1967 version prediction model to 12 summer cases and the analysis of the resulting forecasts, together with the supplementary experimental prediction for the sensitivity of soil moisture and the comparative forecasts with a spectral model, leads to the following conclusions:

1) The July forecasts are overall poorer than the January forecasts. The prediction is inferior for the lower part of the troposphere, suggesting that the physical effects near the earth's surface are complex in summertime.

2) The prediction of the middle troposphere (say, 500 mb height) in July is slightly worse up to 5 days than that in January. But the deterioration beyond 5 days is not severe; the rms skill score remains above persistence for the entire two-week period, and the correlation for height anomalies stays above zero. The difference from the January case in this respect comes from the better forecast of the planetary-scale waves.

3) The July stratospheric prediction was a complete failure with the nine-level model. The tropo-

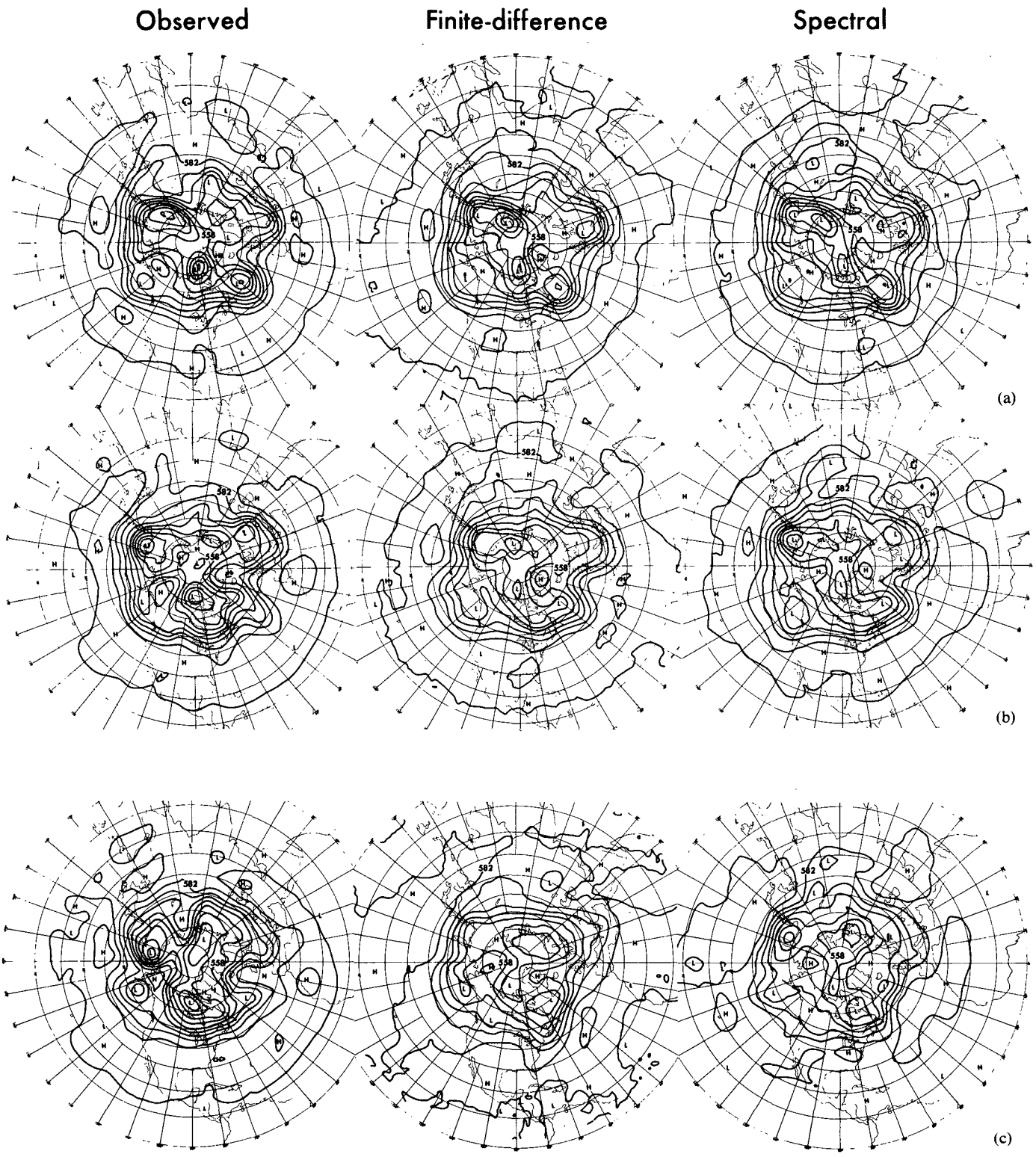

FIG. 23. Height maps at 500 mb for 2, 4 and 8 days, (a)–(c). Left, observation; middle, 1967 version model; right, spectral model (Gordon Stern, 1974). Contours are at 60 m intervals.

TABLE 3. Skill scores of finite difference versus spectral models (three case averages). The first line is the finite-difference model, the second the spectral model and the third persistence.

500 mb geopotential height

	Day										
	1	2	3	4	5	6	7	8	9	10	
rms error (m)	35	44	51	58	67	72	74	77	79	78	Fint.
	35	44	51	59	67	*70*	*70*	*73*	*71*	*73*	Spec.
	44	66	75	80	81	81	82	86	86	87	Pers.
Correlation of Z	0.87	0.78	0.69	0.60	0.48	0.39	0.33	0.24	0.16	0.17	Fint.
	0.86	0.77	0.68	0.59	0.48	*0.45*	*0.41*	*0.36*	*0.37*	*0.30*	Spec.
	0.80	0.55	0.40	0.33	0.34	0.34	0.31	0.24	0.22	0.19	Pers.
Correlation of $\nabla^2 Z$	0.41	0.24	0.17	0.13	0.10	0.07	0.03	0.02	0.00	0.02	Fint.
	0.63	*0.48*	*0.34*	*0.27*	*0.20*	*0.13*	*0.12*	*0.12*	*0.14*	*0.09*	Spec.
	0.52	0.32	0.30	0.26	0.21	0.23	0.24	0.20	0.19	0.18	Pers.
$S1$ United States	0.38	*0.41*	*0.53*	*0.53*	*0.56*	*0.64*	*0.67*	*0.66*	*0.58*	0.60	Fint.
	0.36	0.46	0.55	0.63	0.65	0.71	0.70	0.71	0.63	0.59	Spec.
	0.50	0.59	0.65	0.65	0.68	0.73	0.72	0.71	0.69	0.67	Pers.

1000 mb geopotential height

	Day										
	1	2	3	4	5	6	7	8	9	10	
rms error (m)	34	42	49	52	55	61	60	60	62	65	
	36	43	*43*	*49*	54	*53*	*56*	58	*58*	*60*	
	33	46	54	55	54	55	54	54	55	57	
Correlation of Z	*0.73*	*0.59*	0.47	0.46	0.35	0.20	0.18	0.18	0.09	0.08	
	0.68	0.53	*0.53*	0.45	0.34	*0.30*	*0.24*	*0.22*	*0.20*	*0.19*	
	0.69	0.40	0.19	0.18	0.15	0.08	0.16	0.17	0.14	0.14	
Correlation of $\nabla^2 Z$	0.16	0.09	0.05	0.03	0.02	0.01	0.01	0.00	−0.00	−0.00	
	0.37	*0.21*	*0.15*	*0.10*	*0.05*	0.02	0.02	*0.03*	*0.03*	*0.03*	
	0.40	0.19	0.18	0.17	0.13	0.10	0.11	0.08	0.15	0.15	
$S1$ United States	0.62	0.87	*0.81*	*0.83*	*0.87*	0.96	0.96	0.89	*0.92*	0.90	
	0.63	*0.82*	0.87	0.88	0.97	0.97	0.95	0.98	0.100	0.92	
	0.68	0.92	0.84	0.76	0.82	0.91	0.88	0.82	0.82	0.80	

Italicized values indicate forecasts of better skill score between the two models.

spheric effect has penetrated excessively into the stratosphere.

4) The spectral amplitudes for 1000 mb geopotential height relative to 500 mb height are large during summer compared with those in winter.

5) The regions of the largest prediction errors are the Turkestan area, due to the drawbacks of specified soil moisture and probably the inappropriate treatment of east Asian monsoon, and the Sahara Desert area, due to the deficiency in the specification of the soil moisture.

6) The predicted general circulation features derived by averaging the last 10 days in the two-week forecast period are as follows: The temperature poleward of 30°N in the troposphere is lower than the observed; this is similar to the result for January in Part I. However, the troposphere equatorward of 30°N as well as the stratosphere is higher than the observed, possibly due to the equatorial wall.

The midlatitude westerlies in the troposphere penetrated erroneously into the stratosphere, and the westerlies extended laterally into the doldrums. The eddy kinetic energy is appreciably lower than the observed.

7) Comparing the prediction performance of this model with a spectral model with comparable resolution and physics, it was noticed that the verification series of rms error of the geopotential height, the correlation coefficient of height anomaly and correlation of Laplacian of height anomaly are somewhat worse in the finite-difference model than the spectral model, while the $S1$ score over the United States in the finite-difference model is better than the other.

Acknowledgments. The authors wish to thank Drs. J. Smagorinsky and T. C. Gordon for valuable discussions; Drs. W. Bourke, F. Mesinger and Mr. D. Baumhefner for criticism of the manuscript draft; and Dr. J. Brown for supplying the NMC program to calculate the $S1$ skill score and Messrs. J. Chludzinski, I. Shulman and W. Stern for programming and technical assistance. Gratitude is also expressed to Mrs. B. Williams, Messrs. P. G. Tunison and J. N. Conner for typing and graphical assistance.

REFERENCES

Arakawa, A., 1966: Computational design for long-term numerical integration of the equations of fluid motion: two-dimensional incompressible flow. Part I. *J. Comput. Phys.*, **1**, 119–143.

——, and W. H. Schubert, 1974: Interaction of cumulus cloud ensemble with the large-scale environment, Part I. *J. Atmos. Sci.*, **31**, 674–701.

——, and V. R. Lamb, 1977: Computational design of the basic dynamical processes of the UCLA general circulation model. *Methods in Computational Physics*, Vol. 17, *General Circulation Models of the Atmosphere*, J Chang, Ed., Academic Press, 173–265.

Arpe, K., L. Bengtsson, A. Hollingsworth and Z. Janjić, 1976: A case study of a 10-day prediction. Tech. Rep. No. 1, European Centre for Medium-Range Weather Forecasts, Bracknell, U.K., 105 pp.

Baede, A. P. M., and A. W. Hansen, 1977: A ten-day high-resolution nonadiabatic spectral integration; a comparative study. Tech. Rep. No. 7, European Centre for Medium-Range Weather Forecasts, Bracknell, U.K., 81 pp.

Baer, F., 1972: An alternate scale representation of atmospheric energy spectra. *J. Atmos. Sci.*, **29**, 649–664.

Baumhefner, D., 1976: A single forecast comparison between NCAR and GFDL GCM's. *Mon. Wea. Rev.*, **104**, 1175–1177.

——, and P. Downey, 1976: Forecast intercomparisons between large-scale numerical prediction models. *Ann. Meteor.* (Neue Folge), **11**, 205–208.

——, and ——, 1978: Forecast intercomparisons from three numerical weather prediction models. *Mon. Wea. Rev.*, **106**, 1245–1279.

Blackmon, M. L., 1976: A climatological spectral study of the 500 mb geopotential height of the Northern Hemisphere. *J. Atmos. Sci.*, **33**, 1607–1623.

Bleck, R., 1977: Numerical simulation of lee cyclogenesis in the Gulf of Genoa. *Mon. Wea. Rev.*, **105**, 428–445.

Bourke, W., 1972: An efficient one-level primitive equations spectral model. *Mon. Wea. Rev.*, **100**, 683–699.

Burpee, R. W., 1972: The origin and structure of easterly waves in the lower troposphere of North Africa. *J. Atmos. Sci.*, **29**, 77–90.

Burridge, D. M., and J. Haseler, 1977: A method for medium range weather forecasts—adiabatic formulation. Tech. Rep. No. 4, European Centre for Medium Range Weather Forecasts, Bracknell, U.K., 46 pp.

Carson, D. J., 1978: First results from the GARP Basic Data Set Project. The GARP Programme on Numerical Experimentation, Rep. 17, 38 pp.

Corby, G. A., A. Gilchrist and R. L. Newson, 1972: A general circulation model of the atmosphere suitable for long period integrations. *Quart. J. Roy. Meteor. Soc.*, **98**, 809–833.

Crutcher, H. L., and J. J. Jenne, 1970: An interim note on Northern Hemisphere climatological grid data tape. Department of Commerce, NOAA, Environmental Data Service, National Weather Records Center, 8 pp.

Deardorff, J. W., 1973: Three-dimensional modelling of the planetary boundary layer. *Workshop on Micrometeorology*, D. A. Haugen, Ed., Amer. Meteor. Soc., 271–311.

Delsol, F., K. Miyakoda and R. H. Clarke, 1971: Parameterized processes in the surface boundary layer of an atmospheric circulation model. *Quart. J. Roy. Meteor. Soc.*, **97**, 181–208.

Druyan, L. M., R. C. J. Somerville and W. J. Quirk, 1975: Extended-range forecasts with the GISS model of the global atmosphere. *Mon. Wea. Rev.*, **103**, 779–795.

Egger, J., 1972: Numerical experiments on the cyclogenesis in the Gulf of Genoa, *Beitr. Phys. Atmos.*, **45**, 320–346.

Fjørtoft, R., 1953: On the changes in the spectral distribution of kinetic energy for two-dimensional non-divergent flow. *Tellus*, **5**, 225–230.

Francis, P. E., 1975: The use of a multipoint filter as a dissipative mechanism in a numerical model of the general circulation of the atmosphere. *Quart. J. Roy. Meteor. Soc.*, **101**, 567–582.

Garratt, J. R., 1977: Review of drag coefficients over oceans and continents. *Mon. Wea. Rev.*, **105**, 915–929.

Gauntlett, D. J., D. M. Burridge and K. Arpe, 1977: Comparitive extended range numerical integrations with the E.C.M.W.F. global forecasting model 1: The N24, non-adiabatic experiment. Int. Rep. 6, Res. Dept., European Centre for Medium-Range Weather Forecasts, Bracknell, U.K., 86 pp.

Gordon, C. T., 1976: Verification of the GFDL spectral model. *Weather Forecasting and Weather Forecasts: Models, Systems, and Users*, Vol. 2, Notes from a Colloquium Summer, 1976, conducted jointly by the Advance Study Program, Numerical Weather Prediction Project, and Environmental and Societal Impacts Group of the National Center for Atmospheric Research, 745–762.

——, and W. Stern, 1974: Spectral modelling at GFDL. *The GARP Programme on Numerical Experimentation—Report of the International Symposium on Spectral Methods in Numerical Weather Prediction for GARP*, Copenhagen, WMO, 46–82.

Hayashi, Y., and D. G. Golder, 1977: Space-time spectral analysis of midlatitude disturbances appearing in a GFDL general circulation model. *J. Atmos. Sci.*, **34**, 237–262.

Hembree, G. D., 1977: Comments on "A single forecast comparison between the NCAR and GFDL general circulation models." *Mon. Wea. Rev.*, **105**, 1598–1602.

Hollingsworth, A., 1977: A study of some parameterizations of sub-grid processes in a baroclinic wave in a two-dimensional model. Tech. Rep. No. 5, European Centre for Medium-Range Weather Forecasts, Bracknell, U.K., 45 pp.

Houghton, D. D., and W. S. Irvine, 1976: A case study comparison of the performance of operational prediction models used in the United States. *Mon. Wea. Rev.*, **104**, 817–827.

Jenne, R., 1975: Data sets for meteorological research. NCAR Tech. Note, IA-111, 169 pp.

Kasahara, A., 1977: The effect of mountains on synoptic-scale flows. NCAR Ms. 0901-77-1. [A general review paper presented at the meeting 24–28 October, 1977, Venice, Italy, for GARP Subprogramme on air-flow over and around mountains.]

Klein, W. H., 1957: Principal tracks and mean frequencies of cyclones and anticyclones in the Northern Hemisphere. Res. Pap. No. 40, U.S. Weather Bureau, Washington, DC 60 pp. [NTIS $$$ $$$].

Kuo, H. L., 1952: Three-dimensional disturbances in a baroclinic zonal current. *J. Meteor.*, **9**, 260–278.

Leith, C. E., 1974: Spectral statistical-dynamical forecast experiments. Rep. Int. Symp. Spectral Methods in Numerical Weather Prediction, Copenhagen, Working Group on Numerical Experiment for GARP, WMO, 445–467.

——, 1978: Objective methods for weather prediction. *Annual Reviews of Fluid Mechanics*, Vol. 10, Annual Reviews, Inc., 108–128.

Lilly, D. K., 1967: The representation of small-scale turbulence in numerical simulation experiments. *Pro. IBM Sci. Com-*

puting Symp. Environmental Sciences, Thomas J. Watson Research Center, Yorktown, NY, 195–210.

Manabe, S., 1969: Climate and the ocean circulation. I. The atmospheric circulation and the hydrology of the earth's surface. *Mon. Wea. Rev.*, **97**, 739–774.

——, and J. L. Holloway, Jr., 1975: The seasonal variation of the hydrologic cycle as simulated by a global model of the atmosphere. *J. Geophys. Res.*, **80**, 1617–1649.

——, D. G. Hahn and J. L. Holloway, Jr., 1974: The seasonal variation of the tropical circulation as simulated by a global model of the atmosphere. *J. Atmos. Sci.*, **31**, 43–83.

Mesinger, F., 1977: Forward-backward scheme and its use in a limited area model. *Beitr. Phys. Atmos.*, **50**, 200–210.

——, and A. Arakawa, 1976: Numerical methods used in atmospheric models, Vol. 1. GARP Publ. Ser. No. 17, Joint Organizing Committee GARP, 64 pp.

Miyakoda, K., 1973: Cumulative results of testing a meteorological-mathematical model. The description of the model. *Proc. Roy. Irish Acad.*, **73A**, 99–130.

——, 1975: Weather forecasts and the effects of the sub-grid scale processes. Seminars on Scientific Foundation of Medium-Range Weather Forecasts, Part II, European Centre for Medium-Range Weather Forecasts—ECMWF, Reading, 380–593.

——, and J. Sirutis, 1977: Comparative integrations of global models with various parameterized processes of subgrid scale vertical transports: Description of the parameterizations and preliminary results. *Beitr. Phys. Atmos.*, **50**, 445–487.

——, G. D. Hembree, R. F. Strickler and I. Shulman, 1972: Cumulative results of extended forecast experiments. I. Model performance for winter cases. *Mon. Wea. Rev.*, **100**, 836–855.

——, R. F. Strickler, C. J. Nappo, P. L. Baker and G. D. Hembree, 1971: The effect of horizontal grid resolution in an atmospheric circulation model. *J. Atmos. Sci.*, **28**, 481–499.

NCAR, 1975: Development and use of the NCAR/GCM. A Report of the GCM Steering Committee. NCAR Tech. Note NCAR/TN-101-STR, 177 pp.

Newton, C. W., 1956: Mechanisms of circulation change during a lee cyclogenesis. *J. Meteor.*, **13**, 528–539.

Oort, A. H., and E. M. Rasmusson, 1971: *Atmospheric Circulation Statistics*. NOAA Prof. Pap. 5.

Pettersen, S., 1956: *Weather Analysis and Forecasting*, Vol. 1. 2nd ed., McGraw-Hill, 428 pp.

Phillips, N. A., 1978: A test of finer resolution. Office Note 171, Development Div., National Meteorological Center, National Weather Service, NOAA, 21 pp.

Platzman, G. W., 1961: An approximation to the product of discrete functions. *J. Meteor.*, **18**, 31–37.

Priestley, C. H. B., and R. J. Taylor, 1972: On the assessment of surface heat flux and evaporation using large-scale parameters. *Mon. Wea. Rev.*, **100**, 81–92.

Reed, R. J., and B. A. Kunkel, 1960: The arctic circulation in summer. *J. Meteor.*, **17**, 489–506.

Reitan, C. H., 1974: Frequencies of cyclones and cyclogenesis for North America, 1951–1970. *Mon. Wea. Rev.*, **102**, 861–868.

Sadourny, R., 1975: The dynamics of finite-difference models of the shallow-water equations. *J. Atmos. Sci.*, **32**, 680–689.

Saltzman, B., 1967: On the theory of the mean temperature of the Earth's surface. *Tellus*, **19**, 219–229.

Simmons, A. J., and B. J. Hoskins, 1975: A comparison of spectral and finite-difference simulations of a growing baroclinic wave. *Quart. J. Roy. Meteor. Soc.*, **101**, 551–565.

Smagorinsky, J., 1963: General circulation experiments with the primitive equations: I. The basic experiment. *Mon. Wea. Rev.*, **91**, 99–164.

——, 1969: Problems and premises of deterministic extended range forecasting. *Bull. Amer. Meteor. Soc.*, **50**, 286–311.

Somerville, R. C. J., P. H. Stone, M. Halem, J. E. Hansen, J. S. Hogan, L. M. Druyan, G. Russell, A. A. Lacis, W. J. Quirk and J. Tenenbaum, 1974: The GISS model of the global atmosphere. *J. Atmos. Sci.*, **31**, 84–117.

Stone, P. H., S. Chow and W. J. Quirk, 1977: The July climate and a comparison of the January and July climates simulated by the GISS general circulation model. *Mon. Wea. Rev.*, **105**, 170–194.

Teweles, S. Jr., and H. B. Wobus, 1954: Verification of prognostic charts. *Bull. Amer. Meteor. Soc.*, **35**, 455–463.

Umscheid, L., and P. R. Bannon, 1977: A comparison of three global grids used in numerical prediction models. *Mon. Wea. Rev.*, **105**, 618–635.

Walker, J., and P. R. Rowntree, 1977: The effect of soil moisture on circulation and rainfall in a tropical model. *Quart. J. Roy. Meteor. Soc.*, **103**, 29–46.

Williamson, D. L., 1978: The relative importance of resolution, accuracy, and diffusion in short-range forecasts with the NCAR global circulation model. *Mon. Wea. Rev.*, **106**, 69–88.